COMPARATIVE STUDY OF LOCAL DEFECT CORRECTION AND H-ADAPTIVE METHODS

Daria Koliesnikova, Isabelle Ramière, Frédéric Lebon

COMPARATIVE STUDY OF LOCAL DEFECT CORRECTION AND H-ADAPTIVE METHODS

KOLIESNIKOVA Daria[1,2], RAMIERE Isabelle[1], LEBON Frédéric[2]

[1]CEA, DEN, DEC, SESC, LSC, F-13108 Saint-Paul-Lez-Durance, France

[2]Aix-Marseille University, CNRS, Centrale Marseille, LMA, F-13453 Marseille cedex 13, France

Abstract

The present paper is devoted to a comparative study of mesh-step AMR (adaptive mesh refinement) techniques, generally better adapted for industrial applications. The well-known h-adaptive methods (both remeshing and hierarchical) and the multigrid Local Defect Correction approach are compared in the context of elastostatics for linear quadrangular finite elements. The studied AMR approaches are combined with the recovery-based *a posteriori* Zienkiewicz and Zhu error estimator. The detection of regions requiring refinement is carried out based on different considerations about the maximal permissible element-wise error in an optimal mesh (so-called mesh optimality criterion). Various refinement strategies related to the use of different refinement ratios (uniform or adjusted) are also considered. The quality of a refined mesh is finally appreciated by the verification of both global and local accuracy. So far, the local accuracy is quite never checked in the literature while it is of great importance from an engineering point of view. Numerical examples (academic and industrial) enable to compare the efficiency of each AMR method, especially in terms of CPU time and memory space to reach the given error thresholds. The best numerical choices in term of mesh optimality criterion and refinement strategy are also discussed.

KEYWORDS: Adaptive mesh refinement, h-adaptive methods, local multigrid method, mesh optimality criteria, refinement strategy, local error

1 Introduction

Nowadays adaptive mesh refinement (AMR) techniques are promising numerical tools, extensively used for simulating cutting-edge problems of physics and engineering. Indeed, these problems are often characterized by the presence of local concentrations or singularities, such as discontinuous boundary conditions, concentrated loads, sharp re-entrant corners, cracks, etc. A reliable numerical solution of such problems can be obtained through a fine uniform refinement of the whole domain. This choice, however, is often computationally inefficient. An alternative way is to rely on one of the AMR methods, which enable to reduce the computational effort. It is done by adapting automatically the mesh during computations, enriching it in relatively small regions where the solution is less regular and the error is high.

Among popular state-of-the-art AMR techniques, which aim to reduce the discretization error in $\mathcal{O}(h^p)$ - with h the mesh step and p the degree of interpolation function, at least two main groups can be distinguished: adaptive methods (Fig.1a) and local multigrid methods (Fig.1b).

The goal of adaptive techniques is to provide an optimal global mesh either by nodes relocation (r-adaptivity) [1, 2], or through adjusting the elements size (h-adaptivity: hierarchical and remeshing techniques) [3, 4, 5], or via basis functions degree modification (p-adaptivity) [6, 7], or

by solving an additional problem on a superimposed mesh (s-adaptivity) [8, 9]. The convergence rate and efficiency can be increased significantly by coupling the previously mentioned methods: the exponentially fast convergence of the h-p approach has been shown in [10, 11], the reduced computational cost reached thanks to a h-r coupling is argued in [12, 13], while in [14] the r-adaptivity is preceded by a s-approach to capture the local phenomenon and thus to drive the nodes relocation procedure. An alternative approach to p-adaptive techniques is the so-called Conforming Hierarchical Adaptive Refinement MethodS (CHARMS) [15]. It consists in refining basis functions in a conforming hierarchical way, through a linear combination of basis functions of the same order (p unchanged) determined on refined elements.

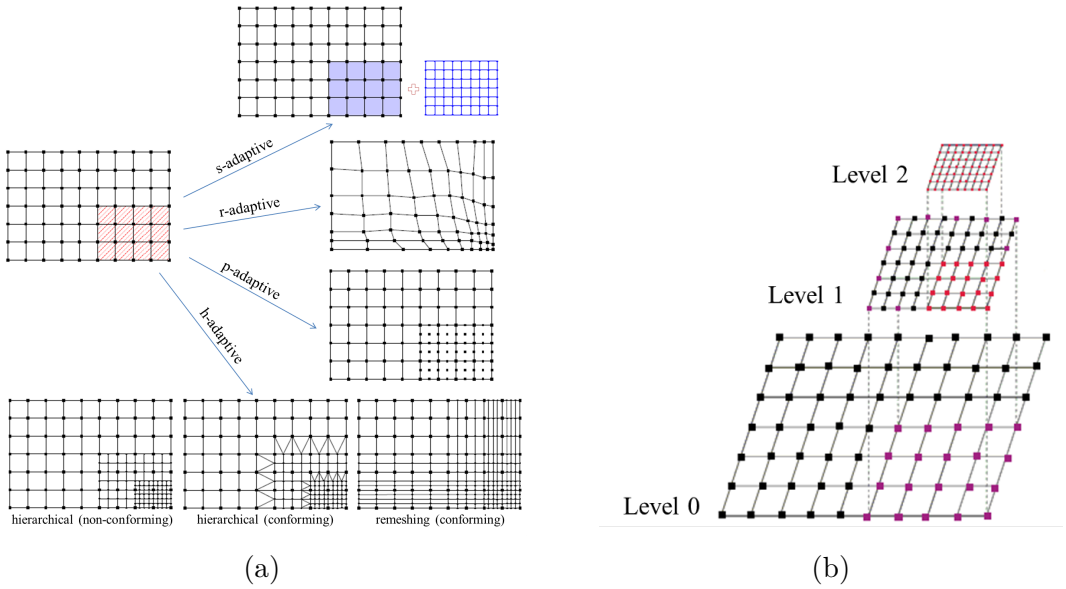

(a) (b)

Figure 1: (a) Adaptive methods: s-, r-, p-, h-refinement approaches; (b) Local multigrid method: example of sub-levels

Local multigrid (or multilevel) methods [16, 17] consist in enriching the solution using solutions defined on separate levels of local meshes, with finer and finer mesh sizes. These techniques can be seen as s- or hierarchical h-adaptive techniques, where the problems defined on each refinement level are solved separately. The generated levels of refinement are linked through an iterative process [18], which allows to transfer information between grids using prolongation and restriction operators. The following main approaches can be mentioned: the Local Defect Correction method [19], consisting in update of the coarse-grid problem's solution with a defect obtained from the restriction of the next finer solution; the Fast Adaptive Composite method [20], based on the simultaneous correction of the coarse and fine problems using a composite residual; or the Flux Interface Correction method [21], relying on the flux conservation between levels of refinement. Among the aforementioned approaches, the most suitable one for solid mechanics problems is the Local Defect Correction (LDC) approach (see [22] for more details).

Strategies based on the adjustment of the elements size (e.g. h-, r-, s-adaptive, CHARMS and local multigrid methods) are generally considered to be more suitable for industrial applications. The p-adaptive approach is limited in this context since industrial solvers are usually designed to treat elements involving basis functions of second order at the most. The main drawback of r-adaptive approach is the limitation in the number of nodes, governed by the initial discretization. In s-adaptive method, all degrees of freedom of generated levels of meshes are solved simultaneously, making this technique similar to the h-adaptive approach, but more expensive than the hierarchical h-adaptive approach. In its turn, the CHARMS technique requires to develop a dedicated solver, whose implementation over existing industrial routines may be really intrusive. Therefore, the goal of the present work is to provide a comparative study of AMR techniques

dedicated to the local refinement of the elements size, which can be easily implementable over existing industrial solvers.

In [23] the comparison of the widely used h-adaptive methods (hierarchical and remeshing) has been performed for second-order triangular finite elements (P2). These techniques, however, have not been deeply compared to the local multigrid LDC method, which also works on the elements size. Thus, we propose here to compare the h-adaptive methods (both, remeshing and hierarchical approaches) to the LDC method in the framework of linear elastostatics. Note that unrefinement is not considered here. In addition, the mesh adaptation over time is beyond of the scope of this paper.

Although in the finite element analysis, the geometry representation has been dominated by the use of triangular elements, a growing interest for quadrilateral meshes appears. It is motivated by the fact that the quadrangular discretization yields more accurate results comparing to the triangular one, since higher order (bilinear) basis functions are involved. Moreover, one can take advantage from the simplicity of the data structure related to the use of quadrangular discretization, which may be beneficially exploited by dedicated linear solvers (regular structured mesh). Hence, in this work, the comparison of previously mentioned AMR techniques will be performed using a linear quadrangular finite elements (Q1) discretization.

In order to guarantee an optimal solution, the mesh refinement procedure should satisfy some basic requirements. First of all, the elements should remain regular and preserve good geometric properties within the whole refinement process [24, 25]. Moreover, it is essential for the mesh generation to require less computational cost than the resolution process itself. Another important feature is that the refinement algorithm has to be as less intrusive as possible, i.e., easily implementable over existing routines in any computational environment. The present study discusses the fulfillment of these requirements by compared AMR techniques.

In general, regions to be refined are not known *a priori*. The use of an *a posteriori* error estimator [26], performed after a computation, allows to automatically identify these regions as well as to provide information about the element-wise error distribution. These ingredients are useful to drive a mesh adaptation procedure. For the sake of pertinent comparative study, the considered AMR strategies are coupled with the same *a posteriori* error estimator: the recovery-based Zienkiewicz and Zhu (ZZ) error estimator [27, 28], known for its robustness and efficiency. Over the years, various criteria (namely mesh optimality criteria) for building the refined mesh (e.g. [27, 29, 30, 31, 32]) based on the estimated error field have been established. After detecting the set of elements to be refined with a chosen criterion we consider in this study three ways to construct an optimal mesh: *(i)* divide the set of detected elements with an *a priori* fixed refinement ratio, so-called fixed-ratio refinement strategy; *(ii)* compute an optimal mesh density function (elements size distribution) for the detected elements using an optimal scaling factor, so-called adjusted-ratio refinement strategy; *(iii)* refine the detected elements with a mean adjusted-ratio, derived from the optimal scaling factor values, so-called mean adjusted-ratio strategy. The first strategy permits to progressively refine the mesh, the aim of the second one is to reach an optimal element size in less remeshing operations but maybe with more elements, while the goal of the third one is to preserve the progressive character of the mesh refinement but using a readjusted uniform refinement ratio.

In the literature, the mesh is defined as optimal when the error of the approximated solution is less than the user-prescribed global accuracy [31]. Following this idea and based on results of the comparative study of [23], the mesh optimality criteria proposed by Zienkiewicz and Zhu in [27] and by Oñate and Bugeda in [29] will be considered for this study. They are both designed to globally fulfill the prescribed accuracy. Although, from the engineering point of view, the most essential feature is to precisely capture localized effects. Thus, the respect of a local prescribed error tolerance is an important component to ensure that the mesh is suitable, in the sense where it permits to concentrate a sufficient number of elements in regions where the solution varies significantly, or where more accurate geometrical representation is needed. To the best of our

knowledge, only in [32] the authors rely on a mesh optimality criterion whose intention is to build a locally optimal mesh. Therefore, in this paper, the mesh optimality criteria are also compared through the final local error verification.

Two numerical examples are considered for this study. First, a benchmark problem of a circular hole in an infinite plate [23], which reveals stress concentrations around the hole, is considered. For this problem, the analytical solution is known. The second test case is derived from nuclear engineering simulations [22, 32, 33]. The studied phenomenon is the so-called mechanical pellet-cladding interaction which is characterized by the presence of a localized stress singularity in the cladding.

The remaining part of this paper is organized as follows: in the next section, the considered AMR strategies (h-adaptive methods, as well as local multigrid LDC approach) are briefly recalled. In Section 3, the ZZ error estimator and the three chosen mesh optimality criteria are described. Section 4 is devoted to numerical results that enable to compare the studied AMR techniques, mainly in terms of the reached accuracy (final global and local errors), number of nodes and CPU time. Finally, conclusions are given.

2 Adaptive mesh-step refinement strategies

Starting from an initial coarse triangulation (or quadrangulation) $\mathcal{T}_0$ of a domain $\Omega \subset \mathbb{R}^D$, an adaptive mesh refinement procedure consists in building a series of triangulations more and more locally refined $\{\mathcal{T}_i\}_{i=0}^k$. The last triangulation $\mathcal{T}_k$ aims to satisfy the prescribed accuracy requirements. At each iteration i, a set of elements which have to be refined $\mathcal{M}_i \subset \mathcal{T}_i$, so-called marked elements, is defined. The set $\mathcal{M}_i$ may be *a priori* detected (user knowledge, geometrical information, etc.) or obtained thanks to an *a posteriori* error estimator (see Section 3). In practice, one defines the set $\mathcal{M}_i^* \subset \mathcal{T}_i$ including the set of marked elements $\mathcal{M}_i$ and eventually elements on which the refinement may be artificially propagated due to methodological features of considered AMR strategies (see the remeshing h-adaptive strategy for example, or a progressive transition zone for the hierarchical h-adaptive technique).

Performing an adaptive mesh-step refinement (except r-approach), the refined mesh $\mathcal{T}_{i+1}$ is obtained by dividing the elements of $\mathcal{M}_i^*$ with a prescribed mesh-step refinement ratio β_{T^i} (which may be assigned to each element T^i of mesh $\mathcal{T}_i$).

Thus, the refinement process tends to create a forest $\mathcal{F}$, having $\#\mathcal{T}_0$ roots, which are the elements $T_{0,j}$ ($j = 1, \ldots, \#\mathcal{T}_0$) of the initial mesh $\mathcal{T}_0$, $\#\mathcal{T}_0$ being the number of elements of $\mathcal{T}_0$. Except the roots, each leaf of the forest $\mathcal{F}$ comes from the refinement of an element from $\mathcal{M}_i^*$. Hence, any element T^i belonging to a set of elements $\mathcal{M}_i^*$ has $\beta_{T^i}^D$ direct successors (children) in $\mathcal{F}$, with D being the dimension of the problem. Moreover, each element (except the roots) has only one predecessor (parent). Thus, the complete triangulation obtained at each refinement iteration $0 \leq i \leq k$ is defined as:

$$\begin{aligned} \mathcal{T}_0 &= \{T_{0,j};\ j = 1, \ldots, \#\mathcal{T}_0\} \quad \text{for } i = 0 \\ \mathcal{T}_i &= \{T^{i-1};\ T^{i-1} \in \mathcal{T}_{i-1} \backslash \mathcal{M}_{i-1}^*\} \bigcup \{T_{i,j};\ j = 1, \ldots, \sum_{T^{i-1} \in \mathcal{M}_{i-1}^*} \beta_{T^{i-1}}^D\} \quad \text{for } 1 \leq i \leq k \end{aligned} \tag{1}$$

The new elements generated at refinement step i by the adaptive refinement procedure are presented as

$$\hat{\mathcal{T}}_i = \{T_{i,j};\ j = 1, \ldots, \sum_{T^{i-1} \in \mathcal{M}_{i-1}^*} \beta_{T^{i-1}}^D\} \tag{2}$$

By definition $\hat{\mathcal{T}}_0 = \mathcal{T}_0$. Elements $T_{i,j}$ are obtained thanks to the division of element $T^{i-1} \in \mathcal{M}_{i-1}^*$ by $\beta_{T^{i-1}}^D$, such that $T_{i,j} \subset T^{i-1}$. To obtain an adaptive refinement as uniform as possible, each edge of T^{i-1} is uniformly divided by $\beta_{T^{i-1}}$. Each element T^i of mesh $\mathcal{T}_i$ represents an element $T_{l,j}$, $0 \leq l \leq i$, $1 \leq j \leq \#\hat{\mathcal{T}}_l$.

2.1 H-adaptive methods

As said in introduction, in the h-version of adaptive methods, the refinement process is performed through the mesh size adjustment. The elements order remains unchanged. It is the number of degrees of freedom that is locally increased to reach the desired precision.

Without loss of generality and by the sake of clarity, we place ourselves in the bi-dimensional case ($D = 2$). While using quadrangular finite elements, three main ways to construct the refined meshes $\{\mathcal{T}_i\}_{i=1}^{k}$ can be considered (cf. Fig.1a). The most natural one consists in directly dividing the marked elements, leading to introducing hanging nodes. This is the hierarchical non-conforming h-adaptive strategy. Another possibility is to add a transition zone (involving triangular elements) in order to avoid the non-conformity of the mesh. This approach is referred as the hierarchical conforming h-adaptive strategy. The third possibility consists in building a conforming mesh composed of quadrangular elements, which implies the necessity to propagate the elements division outside the set of marked elements $\mathcal{M}_i$. This technique is called the remeshing h-adaptive strategy.

For the reasons given in introduction, we limit ourselves to meshes consisting exclusively of quadrangular elements. Thereby, the hierarchical non-conforming as well as the remeshing h-adaptive techniques are considered.

2.1.1 Hierarchical h-adaptive approach

The hierarchical h-adaptive approach can be seen as substituting some coarse mesh elements with finer mesh size patches. The degrees of freedom of the joined parts (refined and non-refined zones) are then solved simultaneously. Thus, at each step i, the refined mesh $\mathcal{T}_i$ (cf. Fig.2a) can be defined by Eq.1.

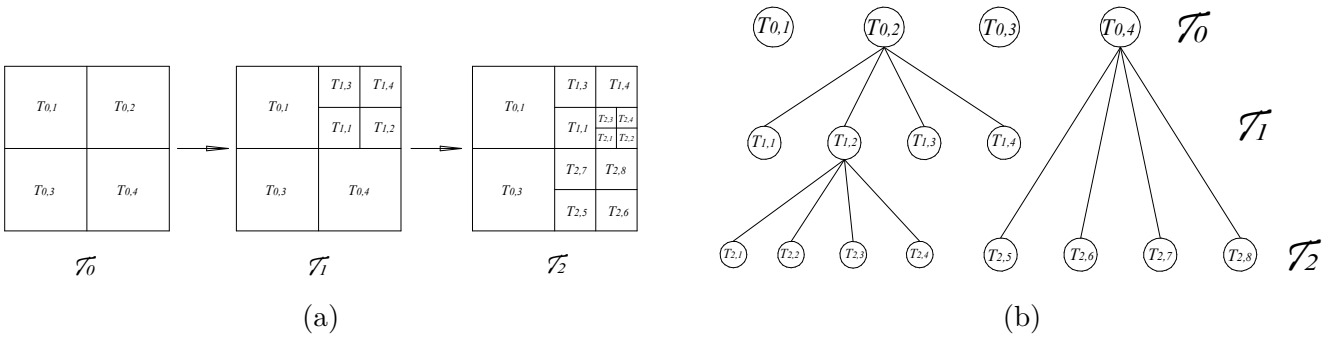

Figure 2: (a) Example of a series of non-conforming gradually refined meshes $\{\mathcal{T}_i\}_{i=0}^{2}$ with the initial triangulation $\mathcal{T}_0 = \{T_{0,j}\}_{j=1}^{4}$, sets of marked elements $\mathcal{M}_0 = T_{0,2}$ and $\mathcal{M}_1 = T_{1,2}$, sets $\mathcal{M}_0^* \backslash \mathcal{M}_0 = \emptyset$ and $\mathcal{M}_1^* \backslash \mathcal{M}_1 = T_{0,4}$, with an uniform refinement factor $\beta = 2$; (b) Forest $\mathcal{F}$ representing meshes $\{\mathcal{T}_i\}_{i=0}^{2}$ with elements of $\mathcal{T}_0$ as the roots.

Generally, the hierarchical h-refinement strategy leads to optimal meshes in terms of number of degrees of freedom. For quadrangular elements, however, hanging nodes appear, which result in a non-conforming mesh. The presence of hanging nodes requires to perform extra algorithmic changes in solver, if it is not dedicated to non-conforming meshes. These modifications are quite intrusive, sometimes challenging to implement and may be consuming in terms of computational time. Several approaches exist to deal with non-conforming meshes: the hanging nodes may be handled using constraint conditions, by introducing Lagrange multiplier [34] or stabilized multiplier [35, 36] methods, by relying on penalty techniques [37, 38], using mortar approach [39, 40], or applying the meshless interpolation [41].

2.1.2 Remeshing h-adaptive approach

The remeshing h-refinement strategy aims to build a conforming mesh consisting of quadrangular elements. In this case, the elements division has to be propagated beyond the set of marked elements $\mathcal{M}_i$ in order to preserve the mesh conformity. The extension leads to set $\mathcal{M}^*$ in Eq.1.

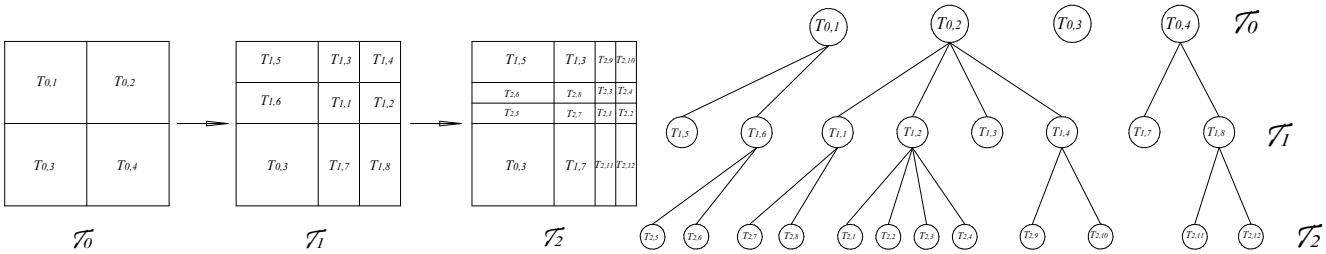

Figure 3: (a) Example of a series of conforming gradually refined meshes $\{\mathcal{T}_i\}_{i=0}^{2}$ with the initial triangulation $\mathcal{T}_0 = \{T_{0,j}\}_{j=1}^{4}$, sets of marked elements $\mathcal{M}_0 = T_{0,2}$ and $\mathcal{M}_1 = T_{1,2}$, sets $\mathcal{M}_0^*\backslash\mathcal{M}_0 = \{T_{0,1} \cup T_{0,4}\}$ and $\mathcal{M}_1^*\backslash\mathcal{M}_1 = \{T_{1,1} \cup T_{1,4} \cup T_{1,6} \cup T_{1,8}\}$, with an uniform refinement ratio on $\mathcal{M}_i$, $\beta = 2$; (b) Forest $\mathcal{F}$ representing meshes $\{\mathcal{T}_i\}_{i=0}^{2}$ with elements of $\mathcal{T}_0$ as the roots.

By imposing the mesh conformity, the refinement is no more completely local. In the case of quadrangular elements, this strategy may rapidly lead to degenerated elements. However, it is easy to deal with resulting conforming meshes since no solver modification is required.

2.2 Local multigrid methods

The idea behind local multigrid methods [42] is to provide a possibility to "zoom" the computational domain in the regions of interest, and to locally improve the accuracy of the solution. This zooming technique permits to capture the local effects without modifying the initial discretization, which allows to implement them in any existing solver in a non-intrusive way.

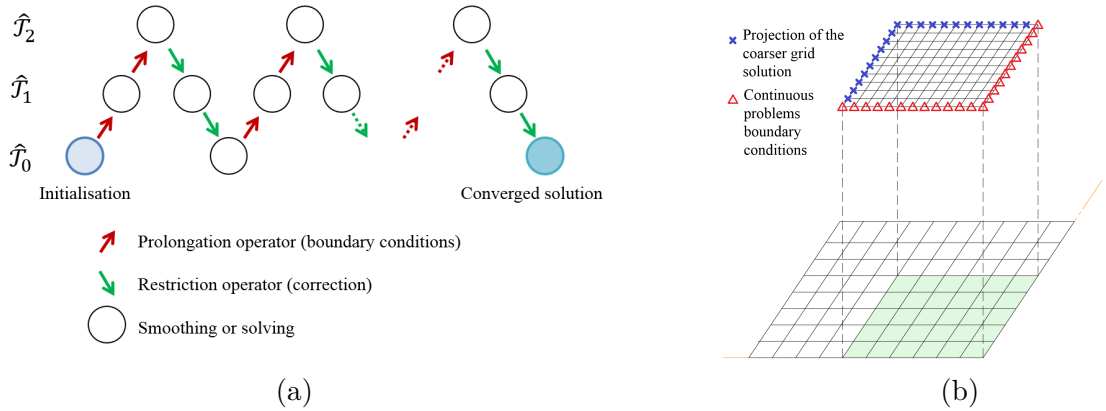

Figure 4: Local multigrid methods: (a) Iterative process; (b) Boundary conditions prolongation of the local multigrid method

In the standard multigrid methods [16] each level is a discretization of whole computational domain, starting from the finest one (except for the Full Multigrid method [16]). In contrast, the local multigrid approaches consist in coarsely meshing the computational domain and in adding finer grids only in local regions where higher precision is needed. Thus, the local multigrid methods can be seen as an inverse standard multigrid method. Problems defined on each generated sub-level are treated in a sequential manner and coupled using an iterative process, lying on prolongation

and restriction operators (see Fig.4a). The prolongation operator is used to prescribe on fictive internal fine mesh boundaries (cf. Fig.4b) the Dirichlet boundary conditions defined from the next coarser solution. The restriction operator enables to update the coarse grid solutions through correction of the coarse problems right-hand side term. The iterative process stops once the solution on the coarsest level is converged. Since during iterations resolution both operators affect problems right-hand side only, operators factorizations can be kept. Thus, the local multigrid process aims to be computationally cheap. In addition, regular and (quasi-)uniform grids can be used on each sub-level leading to the improvement of the problems conditioning. Moreover, local multigrid methods are really generic and flexible as they enable us to change the refinement ratio, the model, the solver, etc. between each sub-level.

For local multigrid methods, Eq.1 describes the composite grid $\mathcal{T}_i$, covering the whole computational domain with locally the most refined elements. In its turn, each $\hat{\mathcal{T}}_i$, $1 \leq i \leq k$, represents one level of generated local grids, see Fig.5. Thereby, in contrast to h-refinement approaches, where the problems to be solved are defined on meshes $\mathcal{T}_i$ (Eq.1), for local multigrid methods the local problems defined on local sub-grids $\hat{\mathcal{T}}_i$ (cf. Eq.2) are considered. Thus, each sub-level i (grid $\hat{\mathcal{T}}_i$) involves only the localized set of marked elements which have been partitioned, leading to small-size problems to be solved separately. Note that in local multigrid methods, the refinement is made in a recursive way, such that

$$\mathcal{M}^*_{i-1} \subset \hat{\mathcal{T}}_{i-1}. \tag{3}$$

Thereby, the composite grid $\mathcal{T}_i$ can be defined in a simpler way as:

$$\mathcal{T}_i = \{T_{l,j};\ l = 0, \ldots, i,\ T_{l,j} \in \hat{\mathcal{T}}_l \setminus \mathcal{M}^*_l\} \quad \text{with } \mathcal{M}^*_i \leftarrow \emptyset \tag{4}$$

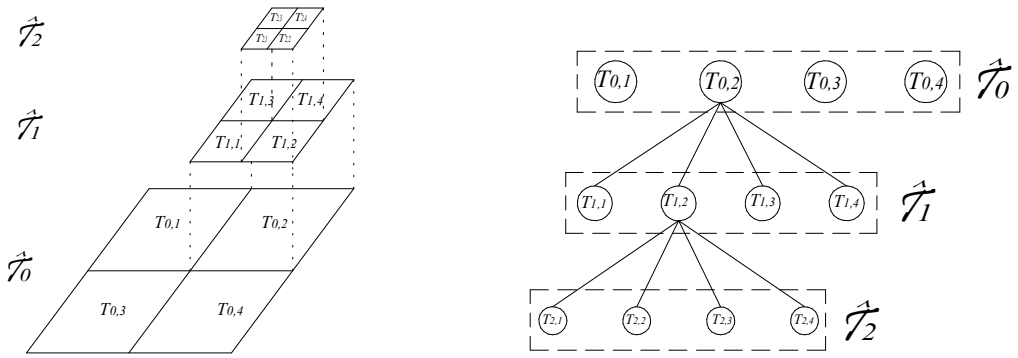

Figure 5: (a) Example of sub-levels of grids $\{\hat{\mathcal{T}}_i\}_{i=0}^2$ with the initial level $\hat{\mathcal{T}}_0 = \{T_{0,j}\}_{j=1}^4$, sets of marked elements $\mathcal{M}_0 = T_{0,2}$ and $\mathcal{M}_1 = T_{1,2}$, sets $\mathcal{M}^*_0 \backslash \mathcal{M}_0 = \emptyset$ and $\mathcal{M}^*_1 \backslash \mathcal{M}_1 = \emptyset$, with an uniform refinement ratio $\beta = 2$; (b) Forest $\mathcal{F}$ representing the meshes $\{\hat{\mathcal{T}}_i\}_{i=0}^2$ with the elements of $\mathcal{T}_0 = \hat{\mathcal{T}}_0$ as the roots.

2.2.1 Local Defect Correction method

As mentioned in introduction, in this study we have chosen to focus on the Local Defect Correction approach, which seems to be the most suitable choice for structural mechanics problems involving the localized effects [22].

The Local Defect Correction technique was initially proposed by Hackbusch in [19]. As for all the existing local multigrid techniques, the prolongation operator of the LDC approach is employed to define the boundary conditions (Fig.4b) of the next finer problem from the next coarser one. The restriction operator serves to derive on the coarse grid a residual (defect) from the fine solution's restriction, and to correct the coarse grid solution using this residual as an

additional source term. The reader is referred to [19] for a more detailed presentation of the LDC algorithm and to [22, 32] for its translation in linear elasticity.

As the LDC algorithm is very generic, it has been successfully applied on various discretization methods to solve a wide range of problems. For example, using finite difference discretization, LDC was applied to combustion in [43], or to convection-diffusion problems in [44]. The use of LDC approach in the framework of finite volume scheme is addressed in [45, 46], and its applicability to the boundary element method is shown in [47]. In the context of finite element method, it has been employed for fluid mechanics problems, see for example [48, 49], and recently for structural mechanics problems in [22, 33, 50].

3 Error estimation and refinement criteria

3.1 Error estimator

A numerical solution of partial differential equations involves various types of errors and inaccuracies, typically the discretization and numerical errors. The discretization error occurs due to the approximation of the solution using a discretization technique (e.g. finite differences, finite elements, finite volumes, etc.). The truncation or round-off error represents the numerical error arising due to the machine precision. Another kind of numerical error may appear due to the iterative resolution of linear systems of equations.

In this paper, the finite element (FE) method is applied and the resulting linear systems of equations are solved using a direct solver. Thus, we assume that the computational error arises mostly from the discretization. Since an exact solution is usually unknown, a real error cannot be computed. Thereby, numerous ways to assess the discretization error have been established, which can be classified into two families: *a priori* and *a posteriori* error estimators. *A priori* estimators (e.g. [51]) are used to characterize the asymptotic behavior of the discretization error (convergence order, etc.). In their turns, *a posteriori* error estimators [26] rely on the computed solution to predict the discretization error.

Currently, three main classes of *a posteriori* error estimators for solid mechanics problems can be cited. Following the pioneering works of Babuška [52], the first class of error estimators is based on the fact that the stress field approximated with FE method generally does not locally verify the equilibrium. This kind of error estimators is referred as residual-based estimators. The second kind of estimators, so-called recovery-based, relies on a recovery procedure [27, 28, 53] to build a smoothed gradient from a discrete one. The third class consists of estimates involving constitutive laws [54, 55] and is based on the construction of a statically admissible stress field.

Usually error estimators are designed to deliver an estimated global error measure as well as an element-wise error distribution. Thus, they are widely coupled to AMR techniques in order to drive automatically the adaptive mesh refinement procedure.

3.1.1 Zienkiewicz and Zhu error estimator

In the framework of linear elasticity, the most generic and widely used error estimator is the recovery-based one proposed by Zienkiewicz and Zhu [27, 28]. As said in introduction, it is the one used in this comparative study. Its key idea is to assess the error as the difference between a reconstructed smoothed gradient $\boldsymbol{\sigma}^*$ and the discrete one $\boldsymbol{\sigma}^h$ (obtained from the computation).

In its first version [27], the recovered (smoothed) stress field $\boldsymbol{\sigma}^*$ is obtained by projection in the following way:

$$\mathbf{M}\boldsymbol{\sigma}^* = \mathbf{b}, \tag{5}$$

with $\mathbf{M} = \int_\Omega (N^T N)\,\mathrm{d}\Omega$, $\mathbf{b} = \int_\Omega (N^T \boldsymbol{\sigma}^h)\,\mathrm{d}\Omega$, with N being the displacement interpolation functions. Here Ω is the computational domain which is represented by the grid $\mathcal{T}_i$ and by the sub-grid

$\hat{\mathcal{T}}_i$ in the case of h-adaptive methods and of the LDC approach respectively.

The improved version appeared in [28], named super-convergent patch recovery (SPR), is based on a polynomial approximation on patches (set of elements having the same vertex):

$$\boldsymbol{\sigma}^* = \mathbf{P}\mathbf{a}, \tag{6}$$

with vector $\mathbf{P}(\boldsymbol{x})$ containing the polynomial terms, and coefficients $\mathbf{a}$ defined by solving a set of linear systems $\mathbf{A}\mathbf{a} = \mathbf{c}$ with $\mathbf{A} = \sum_{i_g=1}^{N_g} \mathbf{P}^T(\boldsymbol{x}_{i_g})\mathbf{P}(\boldsymbol{x}_{i_g})$, $\mathbf{c} = \sum_{i_g=1}^{N_g} \mathbf{P}^T(\boldsymbol{x}_{i_g})\boldsymbol{\sigma}^h(\boldsymbol{x}_{i_g})$, N_g being the total number of superconvergent (Gauss) points contained in the considered patch and $\boldsymbol{x}_{i_g}$ their coordinates.

Whatever the recovery strategy, the element-wise error in the energy norm is estimated as:

$$\|\mathbf{e}\|_{T^i} \simeq \Big(\int_{T^i} (\boldsymbol{\sigma}^* - \boldsymbol{\sigma}^h) : (\boldsymbol{\varepsilon}^* - \boldsymbol{\varepsilon}^h) \, \mathrm{d}T^i \Big)^{\frac{1}{2}}, \tag{7}$$

with $\boldsymbol{\sigma}^h$ and $\boldsymbol{\varepsilon}^h$ - the stress and strain discrete fields, $\boldsymbol{\sigma}^*$ the smoothed stress field and $\boldsymbol{\varepsilon}^*$ the corresponding strain field: $\boldsymbol{\varepsilon}^* = C^{-1}\boldsymbol{\sigma}^*$ (with C being the fourth order elasticity tensor). The global error is then obtained by summing the elementary contributions $\|\mathbf{e}\|_{T^i}$:

$$\|\mathbf{e}\|_{\mathcal{T}_i} = \Big(\sum_{T^i \in \mathcal{T}_i} \|\mathbf{e}\|_{T^i}^2 \Big)^{\frac{1}{2}}. \tag{8}$$

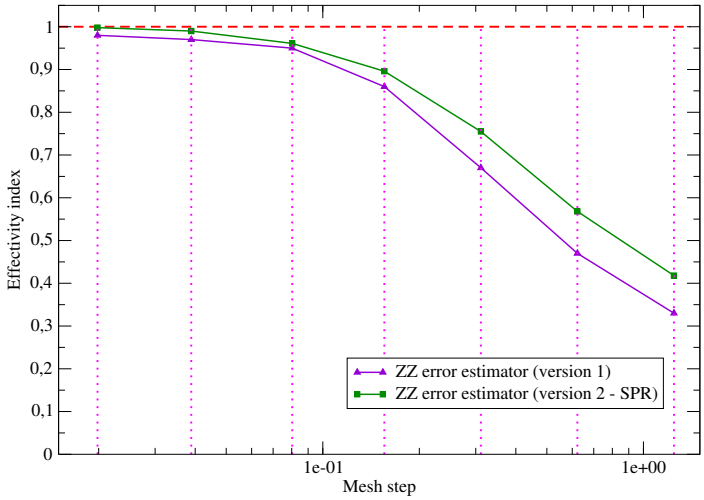

Figure 6: Effectivity index θ vs mesh discretization (plate with circular hole test case [23])

One of the tools which can be used to measure the quality of an error indicator is the effectivity index θ [56], defined as the ratio of the estimated global error $\|\mathbf{e}\|_{\mathcal{T}_i}$ (Eq.8) over the real error $\|\mathbf{e}^{ex}\|_{\mathcal{T}_i}$:

$$\theta = \frac{\|\mathbf{e}\|_{\mathcal{T}_i}}{\|\mathbf{e}^{ex}\|_{\mathcal{T}_i}}, \tag{9}$$

where $\|\mathbf{e}^{ex}\|_{\mathcal{T}_i}$ is computed as $\|\mathbf{e}\|_{\mathcal{T}_i}$ (Eq.8) with $\boldsymbol{\sigma}^* = \boldsymbol{\sigma}^{ex}$ and $\boldsymbol{\varepsilon}^* = \boldsymbol{\varepsilon}^{ex}$ being the exact (or reference) stress and strain fields. An error estimate is called asymptotically exact if its effectivity index tends to one while the mesh size h tends to zero. The two versions of the considered ZZ recovery-based error estimator are good trade-off between reliability and cost. They are easy to implement and robust for a wide range of applications, despite they usually tend to under-estimate the real error ($\theta \leq 1$) (cf. Fig.6).

3.2 Refinement criteria

In an AMR process, the value of estimated global error permits to indicate either a mesh refinement is required or not. Then, the estimated element-wise error distribution is used to determine the local regions to be refined and to predict the elements division ratio.

In the literature [27, 29, 31], the mesh is supposed to be optimal when the tolerance-weighted relative global error measure, defined as

$$\xi_{\mathcal{T}_i} = \frac{\|\mathbf{e}\|_{\mathcal{T}_i}}{\epsilon_\Omega \|\mathbf{w}\|_{\mathcal{T}_i}} \tag{10}$$

is equal to one ($\xi_{\mathcal{T}_i} = 1$). Here ϵ_Ω is an user-specified global error tolerance and $\|\mathbf{w}\|_{\mathcal{T}_i}$ refers to the total strain energy [29] which can be estimated as

$$\|\mathbf{w}\|_{\mathcal{T}_i} \simeq \Big(\int_{\mathcal{T}_i} \boldsymbol{\sigma}^h : \boldsymbol{\varepsilon}^h \, \mathrm{d}\mathcal{T}_i + \int_{\mathcal{T}_i} (\boldsymbol{\sigma}^* - \boldsymbol{\sigma}^h) : (\boldsymbol{\varepsilon}^* - \boldsymbol{\varepsilon}^h) \, \mathrm{d}\mathcal{T}_i \Big)^{\frac{1}{2}}. \tag{11}$$

This global denominator $\|\mathbf{w}\|_{\mathcal{T}_i}$ is close to the energy norm of computed stress field $\boldsymbol{\sigma}^h$. However, one avoids division by zero by adding the second integral.

The refinement of the mesh has to be performed when $\xi_{\mathcal{T}_i} > 1$. As said in introduction, the unrefinement ($\xi_{\mathcal{T}_i} < 1$), interesting for time-dependent problems, is out of the scope of this study.

Various ways to build a new locally refined mesh, called mesh optimality criteria, are available in the literature, see for example [27, 29, 30, 31, 32, 57]. They are based on various considerations about the maximal permissible element-wise error $\|\tilde{\mathbf{e}}\|_{T^i}$. Once this maximal error is defined (see following sections), three strategies to construct a refined mesh are considered in this study:

1. The fixed-ratio refinement strategy, which consists in identifying a set of elements to be partitioned

   $$\mathcal{M}_i = \{T^i \in \mathcal{T}_i; \quad \frac{\|\mathbf{e}\|_{T^i}}{\|\tilde{\mathbf{e}}\|_{T^i}} > 1\}, \tag{12}$$

   and then divide them with an *a priori* fixed uniform refinement ratio β_{T^i}.

   Remark: for the LDC method, as suggested by Eq.3, elements T^i are directly chosen in $\hat{\mathcal{T}}_i$.

2. The adjusted-ratio refinement strategy also aims to define the regions $\mathcal{M}_i$ (Eq.12) and then to compute a new element-size distribution $h_{T_{i+1,j}}$ using an optimal refinement ratio β_{T^i}:

   $$h_{T_{i+1,j}} = \frac{1}{\beta_{T^i}} h_{T^i} \quad \text{for } T^i \in \mathcal{M}_i \quad \text{and } T_{i+1,j} \subset T^i, \tag{13}$$

   where h_{T^i} is the characteristic size of elements T^i of the current mesh $\mathcal{T}_i$. The *a priori* local estimator [27] derived from the classical *a priori* global estimator [51] is generally used to obtain the value of β_{T^i}:

   $$\|\mathbf{e}\|_{T^i} = \mathcal{O}(C_{T^i} h_{T^i}^p) \tag{14}$$

   with $C_{T^i} = C$ being a constant which will be supposed to be independent of the element size and p representing the polynomial order of the discrete basis functions.

   Remark: this strategy is incompatible with the LDC philosophy (i.e. (quasi-)uniform meshes generated by level) and would lead to perform h-adaptive approaches at each level of grid. Hence, this strategy won't be applied to the LDC method.

3. The mean adjusted-ratio refinement strategy aims to refine the elements of $\mathcal{M}_i$ (Eq.12) with an uniform adjusted ratio, derived as follows:

   $$\bar{\beta}_{T^i} = \underset{T^i \in \mathcal{M}_i}{mean} \, \beta_{T^i}. \tag{15}$$

   where β_{T^i} represents an optimal adjusted refinement ratio.

For the present study, three mesh optimality criteria have been chosen to identify $\|\tilde{\mathbf{e}}\|_{T^i}$ and to compute β_{T^i} :

- ZZ criterion based on the equal distribution of the global error [27],
- OB criterion based on the equal distribution of the specific error [29],
- LOC criterion based on the local element-wise error [32].

In [23], authors found that the OB criterion leads to more expensive computations compared to the ZZ criterion without notable improvement of the global error. However, as mentioned in introduction, the chosen criteria have not been compared with regards to the local error, which is generally a more essential aspect for real-life industrial problems. Thus, in this study we will verify which of the selected mesh optimality criteria permits to construct sufficiently refined meshes in order to satisfy the local accuracy requirements too.

3.2.1 Equal distribution of the global error: ZZ criterion

The first considered optimality criterion is the one introduced in [27] by Zienkiewicz and Zhu, namely ZZ criterion. Following the authors idea, the error in the optimal mesh has to be equally-distributed over the elements ($\|\tilde{\mathbf{e}}\|_{T^i} = const. \quad \forall T^i \in \mathcal{T}^i$). The global relative error $\|\tilde{\mathbf{e}}\|_{\mathcal{T}_i}$ (Eq.10) is then defined as:

$$\|\tilde{\mathbf{e}}\|_{\mathcal{T}_i} = \Big(\sum_{T^i \in \mathcal{T}_i} \|\tilde{\mathbf{e}}\|^2_{T^i} \Big)^{\frac{1}{2}} = (\#\mathcal{T}_i)^{\frac{1}{2}} \|\tilde{\mathbf{e}}\|_{T^i}. \tag{16}$$

Since for the optimal mesh $\|\tilde{\mathbf{e}}\|_{\mathcal{T}_i} = \epsilon_\Omega \|\mathbf{w}\|_{\mathcal{T}_i}$, the maximal permissible error per element $\|\tilde{\mathbf{e}}\|_{T^i}$, which is used to define the set of elements requiring partitioning (Eq.12), reads:

$$\|\tilde{\mathbf{e}}\|_{T^i} = \frac{\epsilon_\Omega \|\mathbf{w}\|_{\mathcal{T}_i}}{(\#\mathcal{T}_i)^{\frac{1}{2}}} \tag{17}$$

Consequently, the set of elements assigned for partitioning is determined using Eq.12 with $\|\mathbf{e}\|_{T^i}$ obtained by Eq.7 and $\|\tilde{\mathbf{e}}\|_{T^i}$ defined with the previous expression. One gets the following expression of $\mathcal{M}_i^{ZZ}$:

$$\mathcal{M}_i^{ZZ} = \{T^i \in \mathcal{T}_i; \quad \frac{\|\mathbf{e}\|_{T^i}}{\epsilon_\Omega \|\mathbf{w}\|_{\mathcal{T}_i}} (\#\mathcal{T}_i)^{\frac{1}{2}} > 1\}. \tag{18}$$

In order to get the adjusted refinement ratio β_{T^i}, one assumes the produced mesh $\mathcal{T}_{i+1}$ to be optimal ($\|\mathbf{e}\|_{\mathcal{T}_{i+1}} = \|\tilde{\mathbf{e}}\|_{\mathcal{T}_i} = \epsilon_\Omega \|\mathbf{w}\|_{\mathcal{T}_i}$). Applying Eq.14 for the current mesh $\mathcal{T}_i$ and for the new one $\mathcal{T}_{i+1}$, one gets:

$$\begin{aligned} \|\mathbf{e}\|_{T^i} &= C h^p_{T^i}, \\ \frac{\epsilon_\Omega \|\mathbf{w}\|_{\mathcal{T}_i}}{(\#\mathcal{T}_i)^{\frac{1}{2}}} &= C h^p_{T_{i+1,j}}. \end{aligned} \tag{19}$$

Thus, the following scaling factor $\beta_{T^i}^{ZZ}$ is obtained (from Eq.13):

$$\beta_{T^i}^{ZZ} = \Big(\frac{\|\mathbf{e}\|_{T^i}}{\epsilon_\Omega \|\mathbf{w}\|_{\mathcal{T}_i}} (\#\mathcal{T}_i)^{\frac{1}{2}} \Big)^{\frac{1}{p}} \quad \text{for } T^i \in \mathcal{M}_i^{ZZ}. \tag{20}$$

3.2.2 Equal distribution of the specific error: OB criterion

The second considered criterion is the one based on the equal distribution of the specific error, firstly proposed in [29, 58] by Oñate and Bugeda, referred here as OB criterion. The authors postulate that the optimal element-wise error distribution should be governed by the elements measure. Following this, the ratio between the elementary error's square and the elements measure

must be constant over the whole mesh and equal to the ratio the global error's square over the domain's measure:

$$\frac{\|\tilde{\mathbf{e}}\|^2_{T^i}}{\mu(T^i)} = \frac{\|\tilde{\mathbf{e}}\|^2_{\mathcal{T}_i}}{\mu(\Omega)} \tag{21}$$

with $\mu(T^i)$ being the measure of T^i and $\mu(\Omega)$ - the total measure of computational domain. Similarly to the previous criterion, since in the optimal mesh $\tilde{\xi}_{\mathcal{T}_i} = 1$ (Eq.10), the permissible elementary error reads:

$$\|\tilde{\mathbf{e}}\|_{T^i} = \Big(\frac{\mu(T^i)}{\mu(\Omega)}\Big)^{\frac{1}{2}} \epsilon_\Omega \|\mathbf{w}\|_{\mathcal{T}_i}. \tag{22}$$

Thus, the set of elements to be refined $\mathcal{M}_i^{OB}$ given by the OB criterion is identified in the following way:

$$\mathcal{M}_i^{OB} = \{T^i \in \mathcal{T}_i; \quad \frac{\|\mathbf{e}\|_{T^i}}{\epsilon_\Omega \|\mathbf{w}\|_{\mathcal{T}_i}} \Big(\frac{\mu(\Omega)}{\mu(T^i)}\Big)^{\frac{1}{2}} > 1\}. \tag{23}$$

Considering the adjusted-ratio refinement strategy, Eq.14 gives:

$$\begin{aligned} \|\mathbf{e}\|_{T^i} &= C h^p_{T^i}, \\ \Big(\frac{\mu(T^i)}{\mu(\Omega)}\Big)^{\frac{1}{2}} \epsilon_\Omega \|\mathbf{w}\|_{\mathcal{T}_i} &= C h^p_{T_{i+1,j}}. \end{aligned} \tag{24}$$

Then, the adjusted scaling factor $\beta^{OB}_{T^i}$ is defined as:

$$\beta^{OB}_{T^i} = \Big(\frac{\|\mathbf{e}\|_{T^i}}{\epsilon_\Omega \|\mathbf{w}\|_{\mathcal{T}_i}} \Big(\frac{\mu(\Omega)}{\mu(T^i)}\Big)^{\frac{1}{2}}\Big)^{\frac{1}{p}} \quad \text{for } T^i \in \mathcal{M}_i^{OB}. \tag{25}$$

3.2.3 Local element-wise error: LOC criterion

The alternative third criterion, namely LOC criterion, was briefly mentioned in [29] but effectively introduced and exploited in [32, 33] in the context of structural mechanics problems. It consists in prescribing the local limitation directly on the local element-wise error. The local threshold $\|\tilde{\mathbf{e}}\|_{T^i} = \epsilon_\Omega \|\mathbf{w}\|_{T^i}$ is then used to respect local relative error with $\|\mathbf{w}\|_{T^i}$ computed with Eq.11 over the local elements $T^i \in \mathcal{T}_i$.

In this case, the elements assigned for partitioning are detected in the following way:

$$\mathcal{M}_i^{LOC} = \{T^i \in \mathcal{T}_i; \quad \frac{\|\mathbf{e}\|_{T^i}}{\epsilon_\Omega \|\mathbf{w}\|_{T^i}} > 1\} \tag{26}$$

In a locally optimal mesh, the prescribed local tolerance is supposed to be satisfied in each element ($\|\mathbf{e}\|_{T_{i+1,j}} = \|\tilde{\mathbf{e}}\|_{T^i} = \epsilon_\Omega \|\mathbf{w}\|_{T^i}$). Thus, to define the scaling factor β_{T^i} for this case, one sets:

$$\begin{aligned} \|\mathbf{e}\|_{T^i} &= C h^p_{T^i}, \\ \epsilon_\Omega \|\mathbf{w}\|_{T^i} &= C h^p_{T_{i+1,j}}. \end{aligned} \tag{27}$$

Then, the scaling factor $\beta^{LOC}_{T^i}$ used for the adjusted-ratio strategy reads:

$$\beta^{LOC}_{T^i} = \Big(\frac{\|\mathbf{e}\|_{T^i}}{\epsilon_\Omega \|\mathbf{w}\|_{T^i}}\Big)^{\frac{1}{p}} \quad \text{for } T^i \in \mathcal{M}_i^{LOC}. \tag{28}$$

This criterion aims to ensure the fulfillment of the prescribed local accuracy in each element of the mesh $T^i \in \mathcal{T}_i$. Moreover, as proved in [32], therefore the global prescribed accuracy is also satisfied.

Important remark: It has to be specified, that for the LDC approach or any refinement strategy implying nested refinement zones (see Eq.3), T^i is directly chosen in $\hat{\mathcal{T}}_i$ for the evaluation of $\mathcal{M}_i$ (see Eq.18, 23, 26). However, terms involving $\mathcal{T}_i$ (e.g. $\|\mathbf{w}\|_{\mathcal{T}_i}$, $\#\mathcal{T}_i$, etc.) remain evaluated on the (eventually composite) mesh $\mathcal{T}_i$.

3.3 Stopping criteria

Ideally, the refinement process is stopped automatically when no element needing partitioning is detected: $\mathcal{M}_i = \emptyset$. However, for problems revealing the presence of singularities or local stress concentrations, the previously described criteria may not be self-sufficient to turn off the refinement process. Indeed, $\mathcal{M}_i$ may never become empty. In order to overcome such an issue, additional stopping criteria have to be introduced (see more details in [32]).

Two stopping criteria are used in the present study: the refinement process is finished once both of them hold. The first criterion is the one generally applied to stop AMR processes, which consists in verifying the achievement of the prescribed accuracy globally. At each refinement step, one verifies the condition

$$\xi_{\mathcal{T}_i} \leq 1, \tag{29}$$

where $\xi_{\mathcal{T}_i}$ is the tolerance-weighted relative global estimated error defined by Eq.10. This criterion guarantees an optimal global mesh in the sense of the definition given in [54] but does not give any information about the local error.

Since in the present study we are interested in the local error, an additional local stopping criterion is used. This second criterion, firstly introduced in [32], is based on geometrical considerations. Its main idea is to automatically detect the regions whose refinement becomes inefficient. Indeed, the numerical solution will never converge near a singularity, making the error stagnate (or even increase) while refining the mesh. Thus, the refinement may be stopped when the measure of the set of marked elements $\mathcal{M}_i$ becomes sufficiently small with respect to the measure of whole computational domain:

$$\frac{\mu(\Omega_{\mathcal{M}_i})}{\mu(\Omega)} \cdot 100 \leq \delta \tag{30}$$

where $\mu(\Omega_{\mathcal{M}_i})$ indicates the measure of zone $\Omega_{\mathcal{M}_i} = \{\bigcup \bar{T}^i;\ T^i \in \mathcal{M}_i\}$ and δ is an user-specified parameter (in percent). A value chosen for δ has to be comparatively small in order to guarantee the achievement of desired local accuracy in a dominating part of the domain. For example, the value $\delta = 0.5\%$ was used in [32].

4 Numerical experiments

In this section, the considered AMR approaches are compared on two numerical examples. The studied test cases are implemented through the Cast3M software [59], developed by CEA (French Alternative Energies and Atomic Energy Commission). As already mentioned in introduction, linear quadrangular (Q1) finite elements are used to discretize the problems. Thus, the polynomial order of interpolation functions, used to define the adjusted scaling factor β_{T^i} (Eqs.20, 25, 28), is $p = 1$.

4.1 Numerical considerations

Fixed-ratio refinement strategy

In the case of the fixed-ratio refinement, the uniform scaling factor β_{T^i} is applied to each element assigned for partitioning $T^i \in \mathcal{M}_i$. In this paper, its value is chosen to be equal to two ($\beta_{T^i} = 2$), value usually chosen in practical industrial simulations [22, 33, 60, 61].

Error estimator and refinement criteria

As illustrated in section 3.1.1 (cf. Fig.6), the SPR technique leads to only small improvement of the effectivity index in the case of studied numerical examples. However, this technique is computationally more expensive. Thus, for this study, the first version of the ZZ error estimator (based on projection) is used.

The efficiency of an adaptive mesh refinement procedure obviously strongly depends on the error estimator [31]. Since the ZZ error estimators generally under-estimate the real error (cf. Fig.6), an enlargement of the sets of elements assigned for refinement $\mathcal{M}_i$ is performed while applying each of the studied AMR techniques.

As already discussed in [29], the mesh density function computed using the ZZ criterion may lead to an inconsistent mesh refinement. The elements refined (resp. unrefined) during previous refinement step $i-1$ may be assigned for unrefinement (resp. refinement) at step i, yielding an oscillatory refinement process of some mesh regions. Even if in this study the unrefinement is not allowed, it was decided for ZZ criterion to restrict the detection of the set $\mathcal{M}_i$ of elements to be refined to zone delimited by the previous set $\mathcal{M}_{i-1}$ of marked elements: $\Omega_{\mathcal{M}_i} \subset \Omega_{\mathcal{M}_{i-1}}$. This yields to more and more localized nested refined regions and hence permits to avoid spurious refinement of some zones.

Stopping criteria

In this study, the following global error thresholds are imposed: $\epsilon_\Omega = 2\%, 1\%, 0.5\%, 0.25\%$. The value of parameter δ (Eq.30) used while applying the geometrical stopping criteria is set $\delta = 3\%$ for both numerical examples.

H-adaptive methods

While applying h-adaptive methods, after constructing the new mesh, there exists two ways to perform the computations: either to restart (from scratch) the resolution process, or take advantage of projected information from the preceding mesh to the new one. The second approach is more intrusive but interesting in case of nonlinear problems. The computational cost of the information's transfer may be high and non pertinent in the context of linear elasticity. Thus, it was decided to restart the computations at each refinement step i.

In the case of the hierarchical h-adaptive method, Lagrange multipliers are used to impose interelements continuity (cf. hanging nodes). Moreover, the one-irregularity rule argued in [62, 63] is used. It allows one hanging node per elements edge only. To ensure it, only values $\beta_{T^i} = 2^m$, $m \in \mathbb{N}$ may be prescribed. In addition, some transition zones may be added to $\mathcal{M}_i^*$ (Eq.1) in order to ensure the gradual refinement (cf. Fig.2a).

Local Defect Correction method

The LDC algorithm supposes to define the levels of sub-grids during the first prolongation step in order to perform the iterative process described by the Fig.4a. As the corrected global error is only available after the iterative process convergence, the general LDC algorithm does not enable us to use the first stopping criterion (Eq.29) to turn off the sub-grids generation and hence to stop the refinement process. In order to use this global criterion as for h-adaptive methods, it was decided to rely on a progressive approach as proposed in [64], namely local Full Multigrid (local FMG).

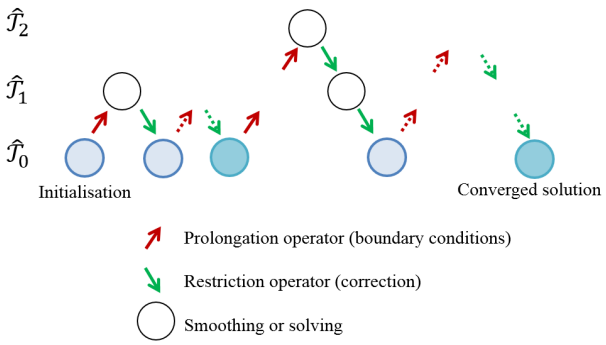

Figure 7: FMG-like iterative process for the LDC method

This technique is very close to the generic LDC algorithm introduced before with the difference that each new sub-level is added after convergence of the iterative process on previously established sub-levels (cf. Fig.7).

During the iterative process, a linear interpolation is used to set the boundary conditions in the prolongation step, while a canonical restriction is employed to restrict the fine-grid solutions to the next coarser grid, since hierarchical nested grids are generated. The chosen operators orders are in agreement with the expected first-order accuracy of the approach. The iterative process is assumed converged when the Euclidean norm relative error between two coarsest level solutions

reaches the prescribed tolerance τ (here $\tau = 10^{-7}$).

In order to keep the LDC algorithm unchanged (generation of one sub-grid with a uniform refinement ratio by level), the adjusted-ratio strategy won't be coupled to the LDC method.

4.2 Methods and criteria comparison

The AMR methods (both remeshing and hierarchical h-adaptive methods as well as LDC method) are compared with regard to the following aspects:

- Number of refinement iterations k (or refinement levels for LDC) performed to meet the prescribed accuracy.
- Relative global exact error $\|\mathbf{e}^{ex}\|^{rel}_{\mathcal{T}_k}$, obtained as follows:

$$\|\mathbf{e}^{ex}\|^{rel}_{\mathcal{T}_k} = \frac{\left(\sum_{T^k \in \mathcal{T}_k} \|\mathbf{e}^{ex}\|^2_{T^k}\right)^{\frac{1}{2}}}{\|\mathbf{w}^{ex}\|_{\mathcal{T}_k}} \tag{31}$$

  where $\|\mathbf{e}^{ex}\|_{T^k}$ and $\|\mathbf{w}^{ex}\|_{\mathcal{T}_k}$ computed using Eq.7 and 11 respectively, with analytical (or reference) solutions $\boldsymbol{\sigma}^* = \boldsymbol{\sigma}^{ex}$ and $\boldsymbol{\varepsilon}^* = \boldsymbol{\varepsilon}^{ex}$.

- Relative local exact error, evaluated quantitatively with the following measure:

$$\eta = \frac{\mu(\Omega_{\mathcal{D}_k})}{\mu(\Omega)} \cdot 100, \tag{32}$$

  where $\mu(\Omega_{\mathcal{D}_k})$ being the measure of $\Omega_{\mathcal{D}_k} = \{\bigcup \bar{T}^k;\ T^k \in \mathcal{D}_k\}$ with $\mathcal{D}_k$ - the set of element where the real local relative error $\|\mathbf{e}^{ex}\|^{rel}_{T^k}$ locally exceeds the prescribed error tolerance: $\mathcal{D}_k = \{T^k \in \mathcal{T}_k;\ \|\mathbf{e}^{ex}\|^{rel}_{T^k} > \epsilon_\Omega\}$. The local relative error is defined as

$$\|\mathbf{e}^{ex}\|^{rel}_{T^k} = \frac{\|\mathbf{e}^{ex}\|_{T^k}}{\|\mathbf{w}^{ex}\|_{T^k}} \tag{33}$$

  where $\|\mathbf{e}^{ex}\|_{T^k}$ (Eq.7) and $\|\mathbf{w}^{ex}\|_{T^k}$ (Eq.11 defined by $T_{k,j}$) are computed with $\boldsymbol{\sigma}^* = \boldsymbol{\sigma}^{ex}$ and $\boldsymbol{\varepsilon}^* = \boldsymbol{\varepsilon}^{ex}$.

  The measure η has to be compared to the local stopping criterion δ. Indeed, an optimal local refined mesh has to meet $\eta \leq \delta$.

- Memory space: total number of nodes being finally stored $N_{tot} = N_{\mathcal{T}_k}$ for h-adaptive methods and $N_{tot} = \sum_{i=0}^{k} N_{\hat{\mathcal{T}}_i}$ for LDC approach, where N_* refers to the number of nodes of corresponding meshes.
- Linear system: maximal size of linear systems to be solved: $N_{max} = \max_i N_{\mathcal{T}_i}$ and $N_{max} = \max_i N_{\hat{\mathcal{T}}_i}$ for h-adaptive methods and for LDC approach, respectively. As unrefinement is not allowed during refinement steps, $N_{max} = N_{\mathcal{T}_k}$ for h-adaptive techniques.
- CPU time: total CPU time including the construction of new global meshes for h-adaptive methods or local sub-grids for the LDC method, the definition and resolution to the problems on the generated refined meshes. For the LDC approach, the time spent during the iterative process is included into the resolution time. Moreover, the time consumptions for problems definition and resolution are explicitly given for each AMR technique.

4.3 Plate with circular hole

The first numerical example is the problem of an infinite plate with a circular hole of radius $R = 1$m, submitted to a prescribed loading $\sigma_\infty = 1$Pa in the $\boldsymbol{e}_1$ direction (cf. Fig.8). The analytical solution of this problem has been provided in [23] and in polar coordinates (r, φ) reads:

$$\begin{aligned}
\sigma_{11}(r,\varphi) &= \sigma_\infty\Big(1 - \frac{R^2}{r^2}\Big(\frac{3}{2}cos2\varphi + cos4\varphi\Big) + \frac{3}{2}\frac{R^4}{r^4}cos4\varphi\Big) \\
\sigma_{12}(r,\varphi) = \sigma_{21}(r,\varphi) &= \sigma_\infty\Big(-\frac{R^2}{r^2}\Big(\frac{1}{2}sin2\varphi + sin4\varphi\Big) + \frac{3}{2}\frac{R^4}{r^4}sin4\varphi\Big) \\
\sigma_{22}(r,\varphi) &= \sigma_\infty\Big(-\frac{R^2}{r^2}\Big(\frac{1}{2}cos2\varphi - cos4\varphi\Big) - \frac{3}{2}\frac{R^4}{r^4}cos4\varphi\Big)
\end{aligned} \tag{34}$$

The material is supposed to be linearly elastic with Young's modulus $E = 10^3\text{N/m}^2$ and Poisson's ratio $\nu = 0.3$. For symmetry reasons, only a quarter of the plate with $a = 10$m is considered, see Fig.8b. Dirichlet boundary conditions expressing the symmetry ($u = 0$) are prescribed on edges I and IV, while values of the analytical solution ($\boldsymbol{\sigma n}$) are imposed on edges II and III.

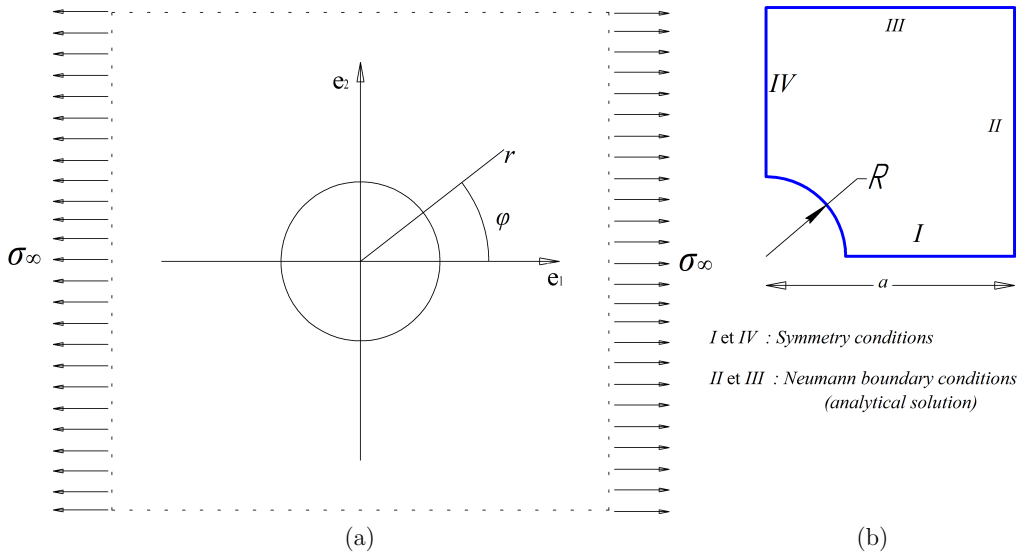

Figure 8: Infinite plate with central circular hole: (a) Sketch of the problem; (b) Computational domain and boundary conditions

To compare the chosen AMR techniques, the same initial coarse triangulation (as uniform as possible) $\mathcal{T}_0$ of the domain Ω is considered. It has to be emphasized, that the domain's discrete boundaries (especially the approximation of the central hole) are updated at each refinement step in order to avoid error's stagnation due to a hole's geometry coarse approximation.

The relative local error maps for various refinement strategy obtained with the ZZ, OB and LOC criteria (for $\epsilon_\Omega = 2\%$) are reported on Fig.9, Fig.10 and Fig.11 respectively. It can be seen that meshes generated by the three refinement methods are similar and refined elements are concentrated in the same zones, here around the central hole, as expected. For the LDC approach, the error maps obtained after convergence of the iterative process are presented on each sub-grid $\{\hat{\mathcal{T}}_i\}_{i=0}^k$ separately and on the composite grid $\mathcal{T}_k$. We can notice that by an automatic mesh refinement procedure, the sets $\mathcal{D}_i$ of elements where the local error exceeds the prescribed tolerance are more and more localized around the central hole. At the end of refinement process, the relative local error respects the accuracy requirements in dominant part of the domain $\mathcal{T}_k \backslash \mathcal{D}_k$ ($(100 - \eta)\%$ of the domain). It can be seen that with OB and LOC criteria the area of the mesh where the local error is controlled is larger (lower η values) than with the ZZ criterion.

Moreover, both OB and LOC criteria allow to satisfy the local error threshold: $\eta \leq \delta$. For a given AMR technique, all refinement strategies (fixed, adjusted and mean ratio) lead to similar results in terms of η value. However, for h-refinement approaches, the final meshes $\mathcal{T}_k$ obtained with the adjusted-ratio strategy after one refinement step ($k = 1$) are more refined compared to these resulting from the fixed-ratio refinement. For the LDC method, the results corresponding to the mean adjusted-ratio strategy are identical to those obtained while applying the fixed-ratio strategy for $\epsilon_\Omega = 2\%$.

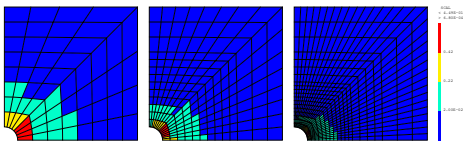

(a) Remeshing h-refinement ($\eta = 4.15\%$) / Fixed-ratio refinement strategy

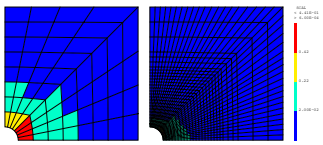

(d) Remeshing h-refinement ($\eta = 3.36\%$) / Adjusted-ratio refinement strategy

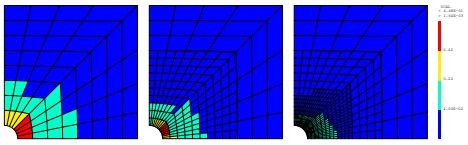

(b) Hierarchical h-refinement ($\eta = 4.15\%$) / Fixed-ratio refinement strategy

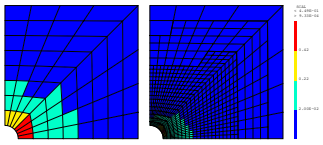

(e) Hierarchical h-refinement ($\eta = 4.15\%$) / Adjusted-ratio refinement strategy

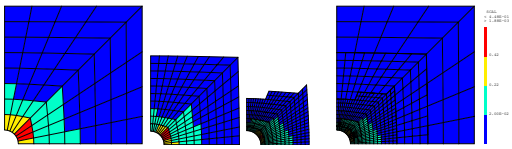

(c) Local Defect Correction ($\eta = 4.15\%$) / Fixed-ratio refinement strategy

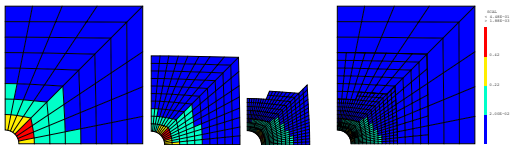

(f) Local Defect Correction ($\eta = 4.15\%$) / Mean adjusted-ratio refinement strategy

Figure 9: Infinite plate with circular hole / local error maps / ZZ optimality criterion / tolerance on the error $\epsilon_\Omega = 2\%$

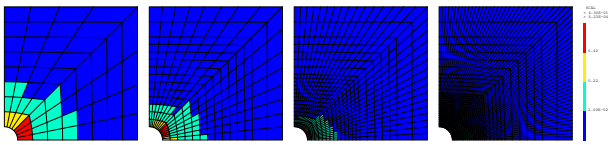

(a) Remeshing h-refinement ($\eta = 2.24\%$) / Fixed-ratio refinement strategy

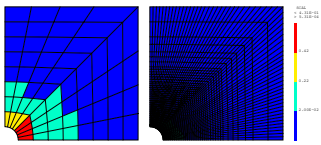

(d) Remeshing h-refinement ($\eta = 2.24\%$) / Adjusted-ratio refinement strategy

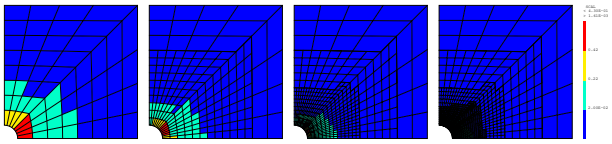

(b) Hierarchical h-refinement ($\eta = 2.24\%$) / Fixed-ratio refinement strategy

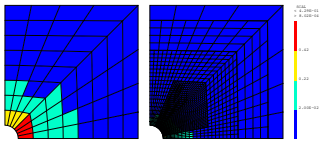

(e) Hierarchical h-refinement ($\eta = 2.84\%$) / Adjusted-ratio refinement strategy

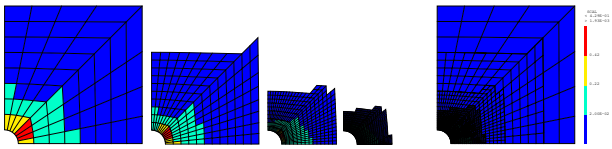

(c) Local Defect Correction ($\eta = 2.24\%$) / Fixed-ratio refinement strategy

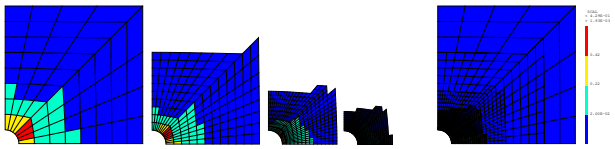

(f) Local Defect Correction ($\eta = 2.24\%$) / Mean adjusted-ratio refinement strategy

Figure 10: Infinite plate with circular hole / local error maps / OB optimality criterion / tolerance on the error $\epsilon_\Omega = 2\%$

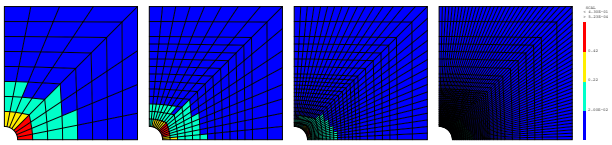

(a) Remeshing h-refinement ($\eta = 2.24\%$) / Fixed-ratio refinement strategy

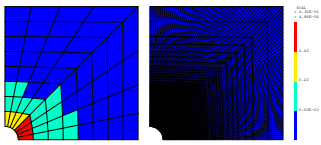

(d) Remeshing h-refinement ($\eta = 1.55\%$) / Adjusted-ratio refinement strategy

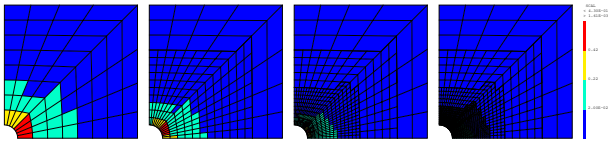

(b) Hierarchical h-refinement ($\eta = 2.24\%$) / Fixed-ratio refinement strategy

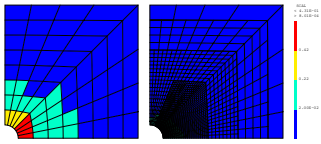

(e) Hierarchical h-refinement ($\eta = 2.42\%$) / Adjusted-ratio refinement strategy

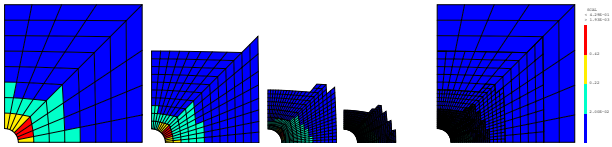

(c) Local Defect Correction ($\eta = 2.24\%$) / Fixed-ratio refinement strategy

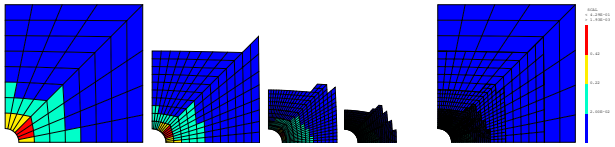

(f) Local Defect Correction ($\eta = 2.24\%$) / Mean adjusted-ratio refinement strategy

Figure 11: Infinite plate with circular hole / local error maps / LOC optimality criterion / tolerance on the error $\epsilon_\Omega = 2\%$

Figure 12 and Table 1 illustrate complementary results obtained with the fixed-ratio strategy. On Figure 12, the real global relative error $\|\mathbf{e}^{ex}\|^{rel}_{\mathcal{T}_k}$ is reported with respect to the total number of nodes N_{tot} and to the total runtime for several user-prescribed tolerance on the error $\epsilon_\Omega = 2\%, 1\%, 0.5\%, 0.25\%$. In Table 1 the results obtained for $\epsilon_\Omega = 0.25\%$ are reported in a more detailed manner. The results corresponding to the uniform refinement (with $\beta_{T^i} = 2$ assigned for all $T^i \in \mathcal{T}_i$) are also shown as reference. The number of refinement iterations k that has to be performed is identical for each refinement method (which is equal to 6 here). Consequently, final meshes with the same minimum mesh-step $h_{T_{k,j}} = \frac{1}{64} h_{T^0}$ are obtained. Each of the considered AMR strategies allow to reach the similar level of accuracy globally with less expensive memory space meshes and faster CPU time, compared to the uniform refinement. The following main differences between the AMR techniques can be mentioned (see Fig.12). The LDC approach is less time consuming compared to h-adaptive techniques, and leads to similar meshes ($N_{\mathcal{T}_k}$) than the hierarchical h-adaptive approach. However, it uses a memory space (N_{tot}) between both h-refinement methods. In counter part, the maximal problem size (N_{max}) to be solved with LDC approach is limited compared to h-adaptive methods, which is beneficial (see the resolution time) especially when using a direct solver. Concerning the mesh optimality criteria, it can be noticed that with the ZZ criterion the local error threshold is exceeded in a larger part of the domain (especially for hierarchical h-adaptive and LDC methods). Moreover, it can be seen on the Figure 12, that the global error tolerance is no longer satisfied for $\epsilon_\Omega = 2\%$ with ZZ criterion coupled to any of the AMR methods. OB and LOC criteria lead to similar results and permit to satisfy the global error tolerance.

Table 1: Infinite plate with circular hole / Fixed-ratio refinement

Tolerance 0.25%	Uniform refinement	Remeshing h-refinement			Hierarchical h-refinement			Local Defect Correction		
		ZZ	OB	LOC	ZZ	OB	LOC	ZZ	OB	LOC
$\|\mathbf{e}^{ex}\|^{rel}_{\mathcal{T}_k}$	0.16%	0.18%	0.17%	0.17%	0.23%	0.21%	0.21%	0.24%	0.21%	0.21%
η, %	2.31	4.47	2.39	2.31	10.85	2.68	2.31	11.05	2.68	2.31
k	6	6	6	6	6	6	6	6	6	6
$N_{\mathcal{T}_k}$	263169	69255	93366	102087	23191	48508	48752	23761	49103	49367
N_{tot}								31323	65119	65453
N_{max}								13207	38817	39123
CPU total	88s	20.4s	27.6s	31.3s	32.1s	51.4s	49.8s	6.7s	20.3s	20.0s
CPU (definition)	1.92s	1.6s	1.9s	2.1s	7.9s	10.6s	10.9s	0.2s	0.3s	0.3s
CPU (resolution)	29.3s	11.5s	15.8s	18.6s	8.3s	12.1s	14.1s	2.3s	6.1s	6.7s

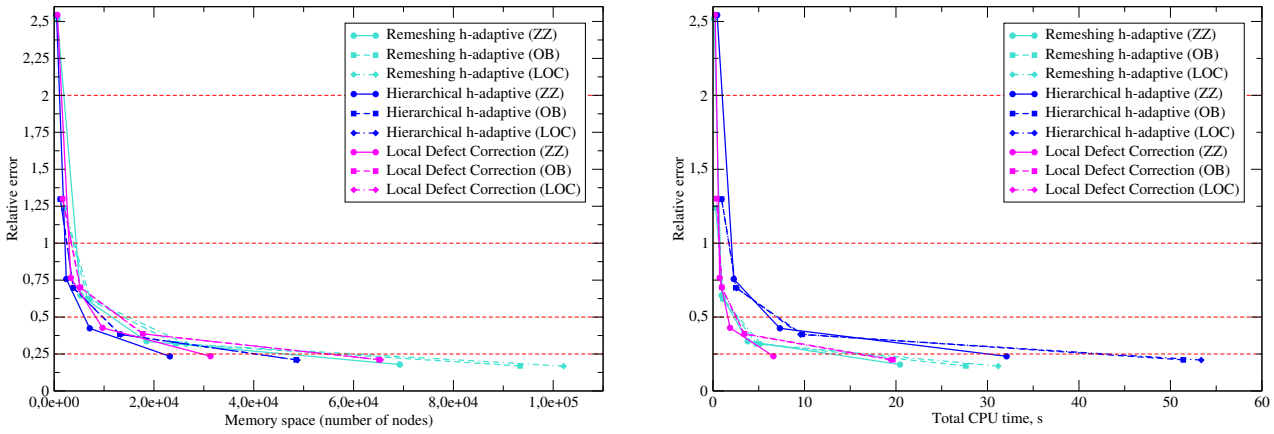

(a) (b)

Figure 12: Infinite plate with circular hole / Fixed-ratio refinement: (a) Relative error vs number of nodes N_{tot}; (b) Relative error vs total CPU time

Table 2 and Figure 13 are dedicated to the adjusted-ratio strategy. It can be seen that more expensive meshes are generated for h-adaptive methods without significant improvement on global and local errors, compared to the fixed-ratio strategy. The total CPU time sometimes even greatly exceeds the time needed for an adapted uniform refinement (for similar $N_{\mathcal{T}_k}$). It is explained by the fact that the adjusted scaling factor β_{T^i} may be excessively high and sometimes inappropriate to meet the required precision (e.g. $max\ \beta_{T^1}^{OB} = 82$ and $max\ \beta_{T^1}^{LOC} = 92$ for $\epsilon_\Omega = 0.25\%$). However, lower scaling factor (e.g. $max\ \beta_{T^1}^{ZZ} = 36$ for $\epsilon_\Omega = 0.25\%$) produced with ZZ criterion sometimes does not permit to satisfy the imposed stopping criteria in one remeshing operation. For the remeshing h-adaptive technique, since the refinement has to be repeated, this could lead to very expensive meshes (e.g. more than 3 millions nodes for $\epsilon_\Omega = 0.25\%$), especially due to the use of quadrangular elements (propagation of the refinement in order to keep the mesh conformity). In this case, computations become too expensive and have not been performed (see Table 2). Thus, the direct use of adjusted scaling factors has to be done with precaution, especially while dealing with problems having localized effects. It has to be mentioned that only OB criterion leads to acceptable results, especially in terms of CPU time. The ZZ and LOC criteria produce too much refined meshes, resulting in expensive (LOC) or even inaccessible (ZZ) computations for low error tolerance (e.g. $\epsilon_\Omega = 0.25\%$). However, for the largest ϵ_Ω value ($\epsilon_\Omega = 2\%$), the global error threshold is exceeded with the ZZ criterion (cf. Figure 13), as also observed for the fixed-ratio strategy.

Table 2: Infinite plate with circular hole / Adjusted-ratio refinement

Tolerance 0.25%	Uniform refinement ($h_{T_{1,j}} = 1/64 h_{T^0}$)	Remeshing h-refinement			Hierarchical h-refinement		
		ZZ	OB	LOC	ZZ	OB	LOC
$\|\mathbf{e}^{ex}\|_{\mathcal{T}_k}^{rel}$	0.16%	-	0.17%	0.12%	0.12%	0.21%	0.19%
η, %	2.31	-	2.44	1.69	4.15	2.82	1.81
k	1	-	1	1	2	1	1
$N_{\mathcal{T}_k}$	263169	-	127946	266794	147070	92361	255697
N_{tot}							
N_{max}							
CPU total	71.5s	-	29.4s	77.1s	364.4s	43.2s	223.7s
CPU (definition)	1.5s	-	0.8s	1.9s	236.4s	15.2s	113.9s
CPU (resolution)	24.2s	-	16.2s	42.8s	59.2s	17.4s	41.5s

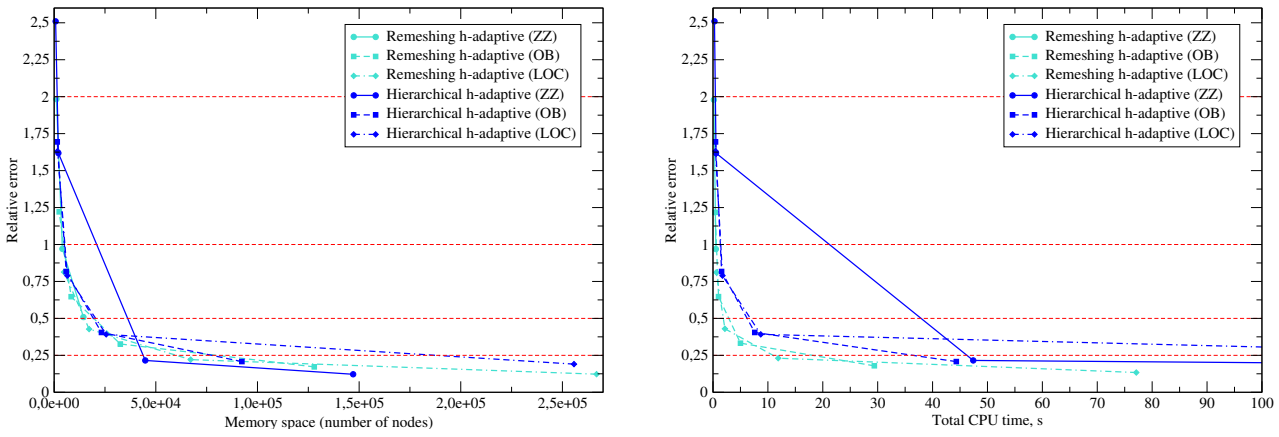

(a) (b)

Figure 13: Infinite plate with circular hole / Adjusted-ratio refinement: (a) Relative error vs number of nodes N_{tot}; (b) Relative error vs total CPU time

The mean adjusted-ratio strategy is applied to the LDC method but also to h-adaptive methods in order to see if excessive refinement is then avoided. The obtained results are reported in the Table 3 and Figure 14. For each AMR method, the mesh is progressively refined, as with the fixed-ratio strategy, but more expensive meshes are generated for a similar final accuracy. However, in this case, these meshes remain less memory consuming than an uniform refinement. Moreover, h-adaptive methods lead sometimes to larger CPU time compared to the uniform refinement (especially for OB and LOC criteria but while respecting the local accuracy). Indeed, in this case, the minimum mesh sizes at the final refinement iteration k for the smallest tolerance $\epsilon_\Omega = 0.25\%$ and for each AMR method are $h^{ZZ}_{T_{k,j}} = \frac{1}{72}h_{T^0}$ (ZZ criterion), $h^{OB}_{T_{k,j}} = \frac{1}{96}h_{T^0}$ (OB criterion) and $h^{LOC}_{T_{k,j}} = \frac{1}{104}h_{T^0}$ (LOC criterion). However, the sufficient minimum mesh step needed to reach the accuracy requirements is $h_{T_{k,j}} = \frac{1}{64}h_{T^0}$ (see the uniform refinement in Table 3, or the fixed-ratio refinement in Table 1). These results may be due to the use of a too coarse initial mesh on which the scaling factor can not be optimally computed. However, it can be noticed that even with the underestimation of the ZZ estimator, the obtained meshes are too refined. A more efficient (in term of effectivity index) error estimator may lead to even more refined meshes. Concerning the mesh optimality criteria, in this case, one can also observe the final global relative error exceeding the user-specified tolerance with the ZZ optimality criterion for $\epsilon_\Omega = 2\%$ (see Figure 14). Once again, the main differences between the AMR strategies, as already discussed for the fixed-ratio refinement, are preserved.

Table 3: Infinite plate with circular hole / Mean adjusted-ratio refinement

Tolerance 0.25%	Uniform refinement ($h_{T_{1,j}} = 1/64 h_{T^0}$)	Remeshing h-refinement			Hierarchical h-refinement			Local Defect Correction		
		ZZ	OB	LOC	ZZ	OB	LOC	ZZ	OB	LOC
$\|\mathbf{e}^{ex}\|^{rel}_{\mathcal{T}_k}$	0.16%	0.16%	0.15%	0.14%	0.19%	0.14%	0.13%	0.19%	0.16%	0.13%
η, %	2.31	4.00	2.11	1.52	7.95	1.79	1.52	8.05	2.35	1.52
k	1	4	3	3	4	3	3	4	3	3
$N_{\mathcal{T}_k}$	263169	92897	133864	266560	29956	116926	130382	30532	70297	129272
N_{tot}								38641	79579	139566
N_{max}								15401	59092	116233
CPU total	71.5s	33.3s	59.7s	174.7s	51.4s	92.6s	120.5s	8.9s	21.3s	43.3s
CPU (definition)	1.5s	1.1s	1.2s	1.8s	17.8s	21.5s	28.6s	0.2s	0.3s	0.5s
CPU (resolution)	24.2s	15.9s	21.8s	19.3s	8.9s	30.5s	37.2s	2.8s	9.2s	12.6s

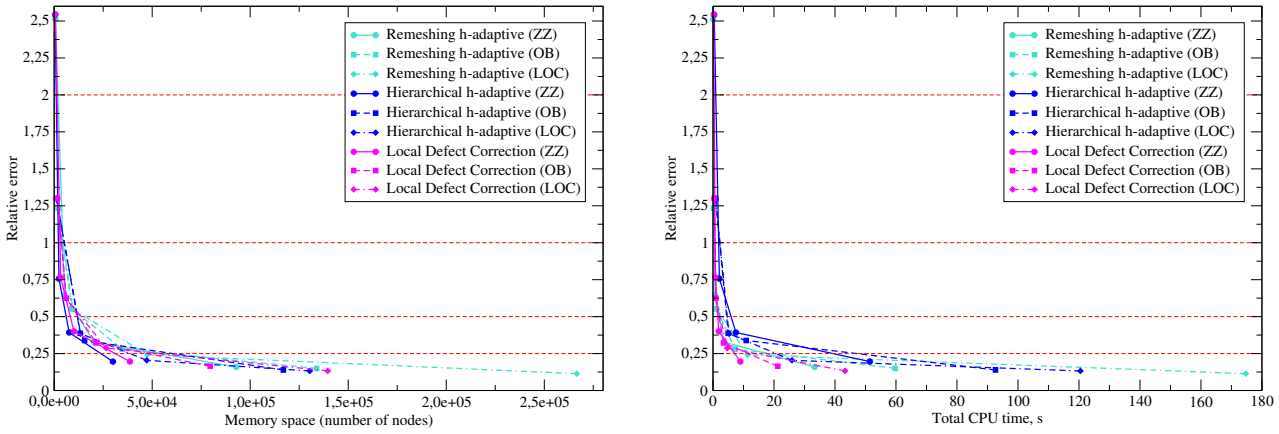

(a) (b)

Figure 14: Infinite plate with circular hole / Mean adjusted-ratio refinement: (a) Relative error vs number of nodes N_{tot}; (b) Relative error vs total CPU time

The comparison of the three mesh optimality criteria is performed with regard to the local error. Evolution of the local error measure η with respect to the required accuracy is illustrated on Figures 15, 16 and 17 for fixed-ratio, adjusted-ratio and mean adjusted-ratio strategies, respectively. It can be seen that the ZZ optimality criterion does not permit to construct sufficiently refined meshes in order to locally satisfy the required accuracy (imposed $\delta = 3\%$ value). For each strategy and each AMR technique, the regions where the local error exceeds the user-prescribed accuracy are greater compared to OB and LOC criteria. Concerning OB and LOC criteria, for this numerical example, they lead to the comparable results (similar η value) with really satisfactory values of η. Thus, these criteria may be recommended for more realistic industrial applications.

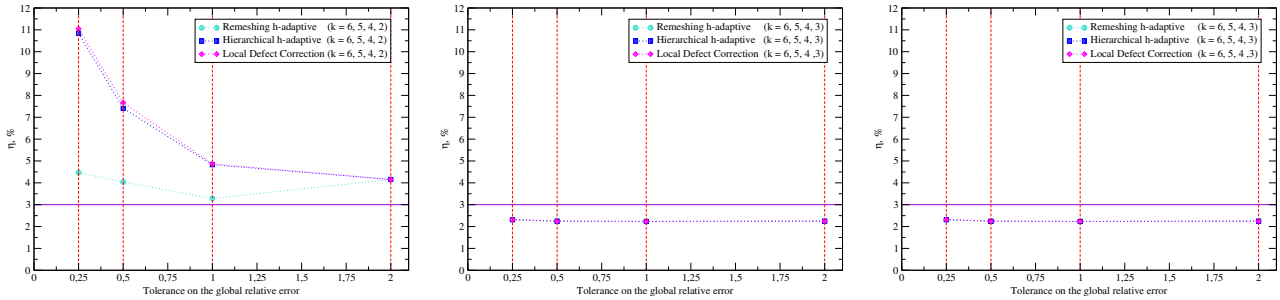

(a) (b) (c)

Figure 15: Infinite plate with circular hole / Fixed-ratio refinement: (a) ZZ optimality criterion; (b) OB optimality criterion; (c) LOC optimality criterion

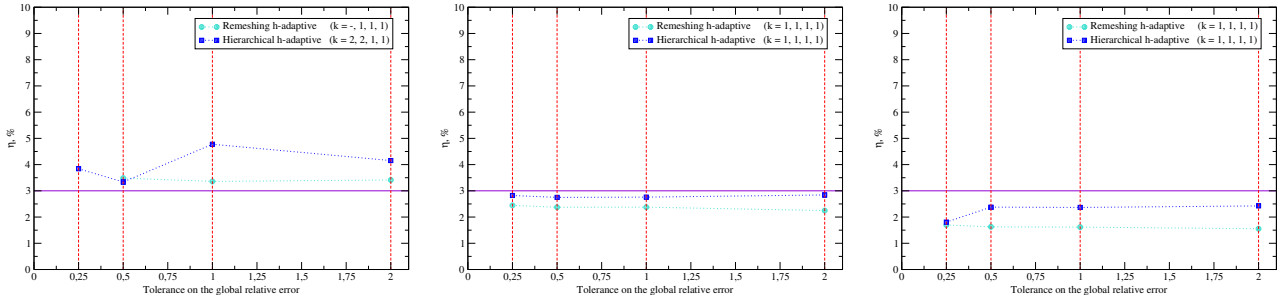

(a) (b) (c)

Figure 16: Infinite plate with circular hole / Adjusted-ratio refinement: (a) ZZ optimality criterion; (b) OB optimality criterion; (c) LOC optimality criterion

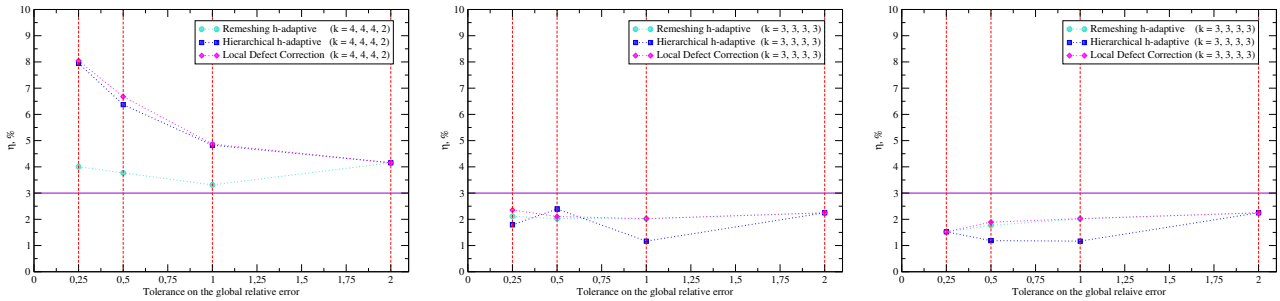

(a) (b) (c)

Figure 17: Infinite plate with circular hole / Mean adjusted-ratio refinement: (a) ZZ optimality criterion; (b) OB optimality criterion; (c) LOC optimality criterion

This numerical example shows that the fixed-ratio strategy (with $\beta_{T^i} = 2$) should be preferred to the adjusted-ratio or mean adjusted-ratio strategies. The fixed-ratio strategy permits to reach the prescribed accuracy more precisely in a progressive way limiting the total final number of nodes. Moreover, the computational time is often optimal even if more remeshing iterations are performed (or more sub-levels are generated).

Hierarchical h-adaptive and LDC methods lead to similar results in terms of generated meshes. The composite grid of LDC approach has almost the same number of nodes as the final mesh obtained with the hierarchical h-refinement method. Both hierarchical h-adaptive and LDC techniques use always more limited memory space than the remeshing h-adaptive method. The remeshing h-refinement yields more expensive and often degenerated meshes. In fact, the necessity to propagate the elements refinement implies the division of elements only in one direction far from the regions where the refinement is required.

Regarding the CPU time, for the remeshing h-adaptive method the time needed to build the sequence of meshes can dominate the total runtime. This can be explained by the need to completely update the mesh of the whole domain at each iteration i. Concerning the hierarchical h-adaptive method, the necessity to menage non-conformity relations requires dedicated algorithms, which make the implementation more intrusive. Moreover, we notice that the time used for problems definition is comparable to the time of solving these problems. This time comes from the additional unknowns and relations which have to be taken into account. Concerning the LDC method, the total runtime is always limited compared to h-adaptive methods. The total CPU time needed to the LDC approach to reach the same level of accuracy is 25 to 45% less compared to the remeshing h-refinement approach, and 30 to 60% less compared to the hierarchical h-adaptive method. Indeed, the possibility of the LDC algorithm to add only local conforming sub-grids allows us to use the existing solver as a black-box. Usually, the generated grids are uniform or quasi-uniform, and consist of a limited number of elements which lead to fast resolution. In addition, the use of uniform grids may open the way to use fast dedicated solvers.

4.4 Industrial test case: mechanical Pellet-Cladding Interaction

The second numerical example is derived from nuclear simulations. The Pellet-Cladding interaction (so-called PCI) is part of a wide range of physical and mechanical phenomena occurring in Pressurized Water Reactor (PWR) during irradiation. In 2D, two test cases are usually used to separately model the two phenomena (the hourglass deformation and the pellets fragmentation) characterizing the PCI, as proposed in [22, 32].

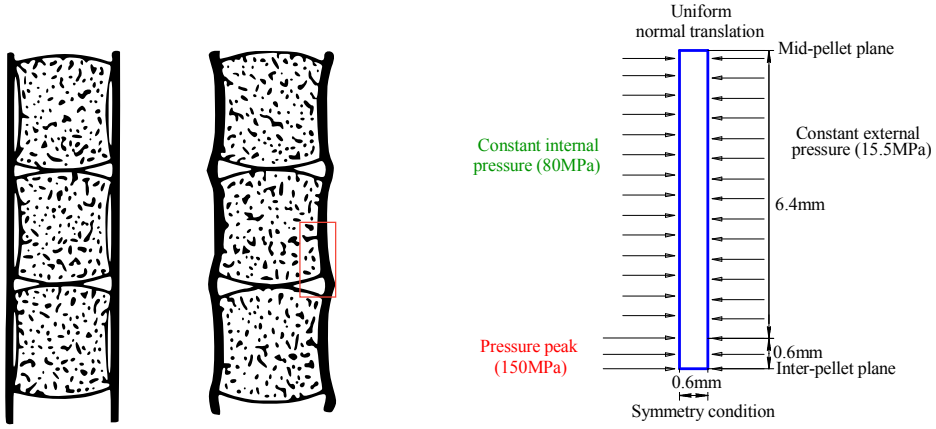

Figure 18: Industrial test case: Pellet-Cladding Interaction. (a) Hourglass shape deformation; (b) Computational domain and boundary conditions for the bi-dimensional axisymmetric test case

In this study, we focus on modeling the cladding's response to the pellet's hourglass deformation, sketched in Fig.18a. The contact is modeled as a discontinuous pressure applied on the the cladding's internal part (cf. Fig.18b). For symmetry reasons, only a half of the pellet's height is represented. A bi-dimensional axisymmetric formulation is assumed. In order to allow an overall normal displacement of the cladding, an uniform normal (*a priori* unknown) translation condition

is assumed at the median plane (top of the modeled domain). The cladding's material is supposed to be linear elastic with Young's modulus $E = 100$GPa and Poisson ratio $\nu = 0.3$. This test case reveals a local singularity in stress (of order 0.5) near the pressure discontinuity zone, cf. [32].

Since the analytical solution of this problem is unknown, the solution obtained using a very fine uniform discretization adapted to the pressure discontinuity with a mesh-step of approximately 2.8μm ($\simeq 1 \cdot 10^6$ nodes) is considered as reference solution.

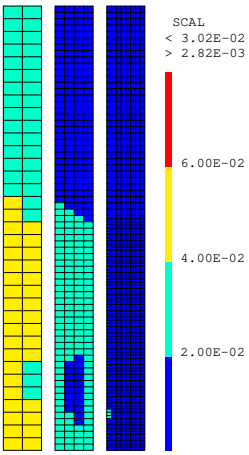

(a) Remeshing h-refinement ($\eta = 0.26\%$) / Fixed-ratio refinement strategy

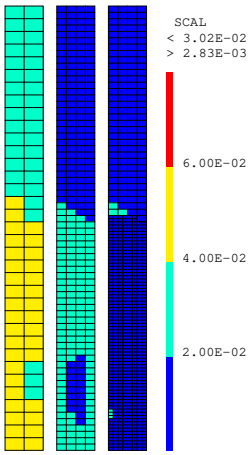

(b) Hierarchical h-refinement ($\eta = 1.33\%$) / Fixed-ratio refinement strategy

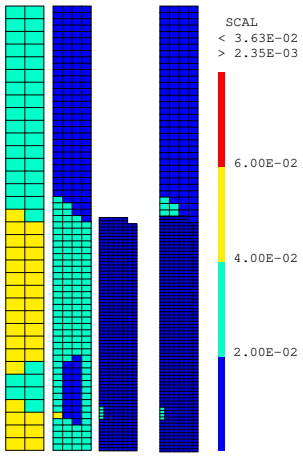

(c) Local Defect Correction ($\eta = 2.14\%$) / Fixed-ratio refinement strategy

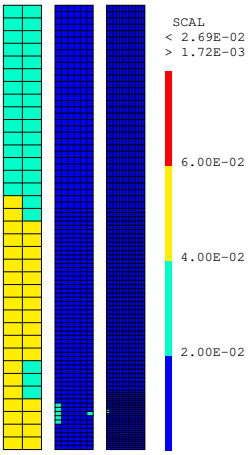

(d) Remeshing h-refinement ($\eta = 0.08\%$) / Adjusted-ratio refinement strategy

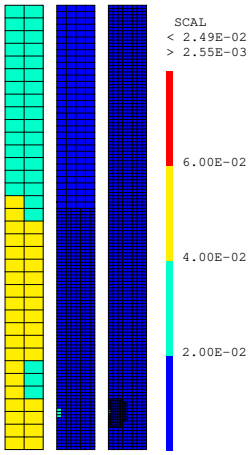

(e) Hierarchical h-refinement ($\eta = 0.05\%$) / Adjusted-ratio refinement strategy

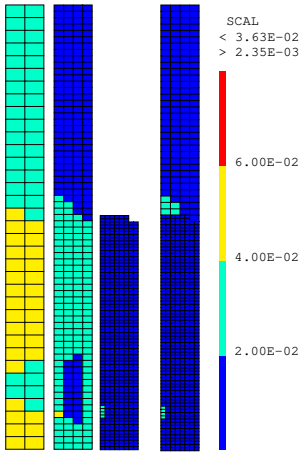

(f) Local Defect Correction ($\eta = 2.14\%$) / Mean adjusted-ratio refinement strategy

Figure 19: Mechanical Pellet-Cladding Interaction / local error maps / ZZ optimality criterion / tolerance on the error $\epsilon_\Omega = 2\%$

The generation of the series of refined meshes $\{\mathcal{T}_i\}_{i=0}^k$ starts from the initial coarse mesh $\mathcal{T}_0$ fitted on the pressure discontinuity (to keep the expected first order convergence in stress, see [65]). In order to verify the previous conclusions obtained on an academic test case, the same simulations methodology is followed here. The relative local error maps obtained using ZZ, OB and LOC criteria for $\epsilon_\Omega = 2\%$ are presented on Figures 19, 20 and 21. The figures show that similar regions are refined whatever the AMR method, and that the refined regions progressively focus around the pressure discontinuity. It can be noticed that whatever the mesh optimality criterion, the refinement strategy and the AMR method, the desired local accuracy ($\eta \leq \delta$) is

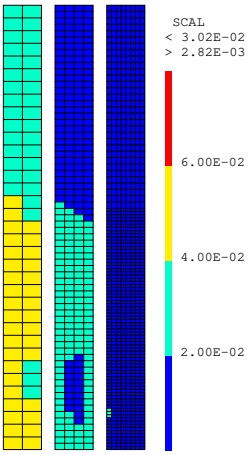

(a) Remeshing h-refinement ($\eta = 0.26\%$) / Fixed-ratio refinement strategy

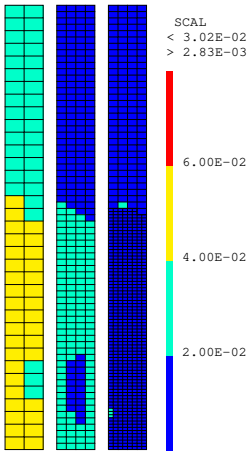

(b) Hierarchical h-refinement ($\eta = 0.62\%$) / Fixed-ratio refinement strategy

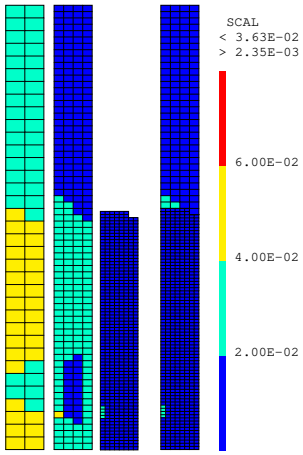

(c) Local Defect Correction ($\eta = 1.42\%$) / Fixed-ratio refinement strategy

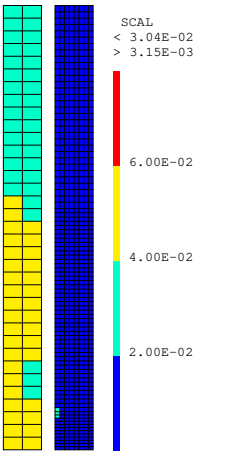

(d) Remeshing h-refinement ($\eta = 0.29\%$) / Adjusted-ratio refinement strategy

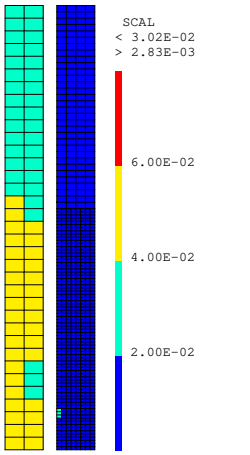

(e) Hierarchical h-refinement ($\eta = 0.26\%$) / Adjusted-ratio refinement strategy

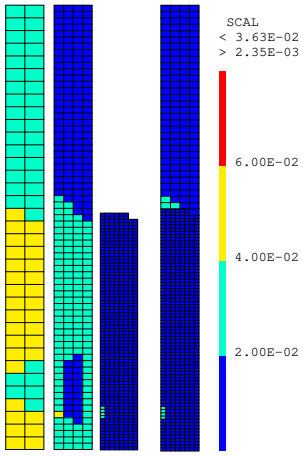

(f) Local Defect Correction ($\eta = 1.42\%$) / Mean adjusted-ratio refinement strategy

Figure 20: Mechanical Pellet-Cladding Interaction / local error maps / OB optimality criterion / tolerance on the error $\epsilon_\Omega = 2\%$

reached for this error threshold. Similarly to the first numerical example, the OB and LOC mesh optimality criteria lead to locally more precise simulations (lower η values) compared to the ZZ criterion.

One can observe that while applying the fixed-ratio strategy (and even the mean-ratio strategy for LDC method), the local accuracy is not satisfied on some elements not detected at the last level of refinement. It occurs mostly due to the under-estimation of the real error by the ZZ error estimator. Such an issue is compensated by the more local LOC optimality criterion, resulting in the improvement of the local error's measure η. It has to be noticed, that with the adjusted-ratio refinement strategy applied to h-adaptive techniques, such situation is no more observed.

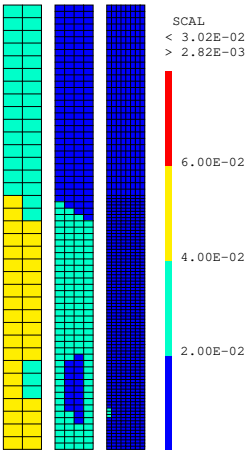

(a) Remeshing h-refinement ($\eta = 0.26\%$) / Fixed-ratio refinement strategy

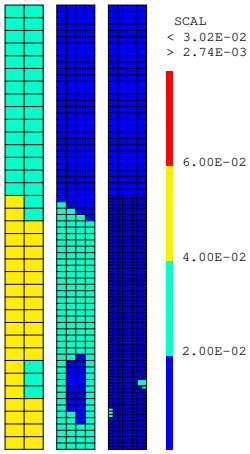

(b) Hierarchical h-refinement ($\eta = 0.71\%$) / Fixed-ratio refinement strategy

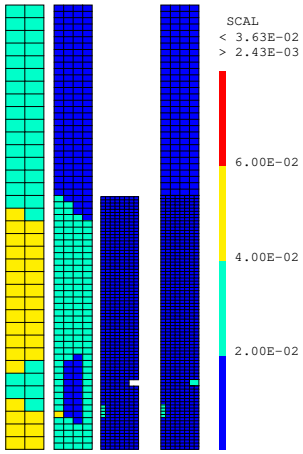

(c) Local Defect Correction ($\eta = 0.71\%$) / Fixed-ratio refinement strategy

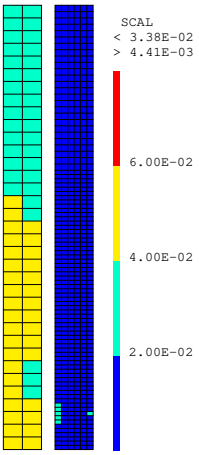

(d) Remeshing h-refinement ($\eta = 0.95\%$) / Adjusted-ratio refinement strategy

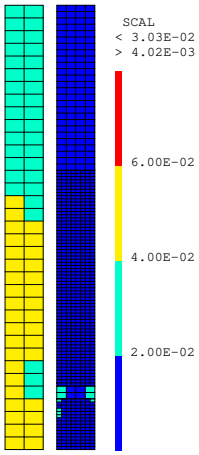

(e) Hierarchical h-refinement ($\eta = 1.87\%$) / Adjusted-ratio refinement strategy

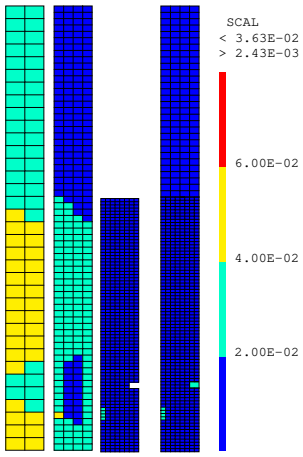

(f) Local Defect Correction ($\eta = 0.71\%$) / Mean adjusted-ratio refinement strategy

Figure 21: Mechanical Pellet-Cladding Interaction / local error maps / LOC optimality criterion / tolerance on the error $\epsilon_\Omega = 2\%$

The results of the fixed-ratio strategy are presented in Table 4 for the error tolerance threshold set to $\epsilon_\Omega = 0.25\%$. The finest mesh steps obtained with all AMR techniques is $h_{T_{k,j}} = \frac{1}{32} h_{T^0}$ ($k = 5$), and is equal to the final mesh step reached with an uniform refinement. In this case, one can observe that the time spent while applying the remeshing h-refinement method is twice greater than performing an uniform refinement. CPU times for the hierarchical h-refinement technique are similar to uniform refinement calculation times. Only the LDC approach is interesting here in term of total runtime. Concerning the memory space, all AMR techniques lead to quite similar outcomes, which results in saving about 2/3 of the place required by an uniform refinement. The reached global relative error with respect to the total number of nodes as well as to the total CPU time is depicted on the Figure 22 for each ϵ_Ω. It can be observed that, whatever the AMR method and optimality criteria, the relative global errors thresholds are respected. Moreover, one can see that all the refinement techniques lead to comparative results in terms of the memory space for each of the imposed ϵ_Ω value, with slightly lower values for the hierarchical h-refinement method. In terms of CPU time, the LDC technique confirms to be the most efficient approach.

Table 4: Mechanical Pellet-Cladding Interaction / Fixed-ratio refinement

Tolerance 0.25%	Uniform refinement	Remeshing h-refinement			Hierarchical h-refinement			Local Defect Correction		
		ZZ	OB	LOC	ZZ	OB	LOC	ZZ	OB	LOC
$\|\mathrm{e}^{ex}\|^{rel}_{\mathcal{T}_k}$	0.09%	0.13%	0.13%	0.13%	0.18%	0.18%	0.18%	0.18%	0.18%	0.18%
η, %	0.13	0.13	0.13	0.13	5.36	5.21	1.36	6.78	6.73	3.26
k	5	5	5	5	5	5	5	5	5	5
$N_{\mathcal{T}_k}$	165249	56160	56875	57395	43338	43497	45318	42337	42484	44275
N_{tot}								58394	58614	61062
N_{max}								33372	33592	36040
CPU total	33.6s	69.1s	69.8s	64.6s	27.9s	28.6s	28.9s	15.9s	16.4s	17.3s
CPU (definition)	0.8s	0.8s	0.8s	0.8s	5.6s	3.3s	3.1s	0.3s	0.3s	0.3s
CPU (resolution)	24.1s	11.6s	12.4s	12.4s	9.5s	8.7s	7.7s	5.1s	5.5s	4.1s

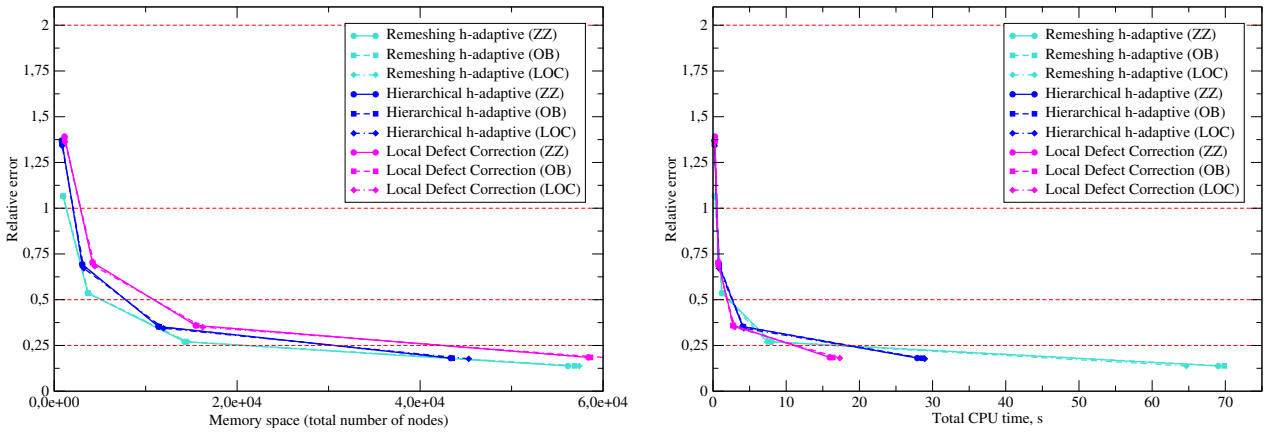

(a) (b)

Figure 22: Mechanical Pellet-Cladding Interaction / Fixed-ratio refinement: (a) Relative error vs number of nodes N_{tot}; (b) Relative error vs total CPU time

Table 5 and Figure 23 correspond to the results obtained with the adjusted-ratio refinement strategy. One can notice that more expensive computations in terms of memory space and CPU time have to be performed compared to the fixed-ratio strategy and to an uniform refinement, especially for the remeshing h-adaptive technique. It is still due to a badly estimated adjusted scaling factor β_{T^i}, whose values are locally excessively high and lead to expensive meshes to be generated. The remeshing h-refinement technique becomes in this case really inefficient. Thus, as for the previous numerical test case, one may conclude that the direct application of the literature adjusted scaling factor has to be avoided.

Table 5: Mechanical Pellet-Cladding Interaction / Adjusted-ratio refinement

Tolerance 0.25%	Uniform refinement ($h_{T_{1,j}} = 1/32 h_{T^0}$)	Remeshing h-refinement			Hierarchical h-refinement		
		ZZ	OB	LOC	ZZ	OB	LOC
$\|\mathbf{e}^{ex}\|^{rel}_{\mathcal{T}_k}$	0.09%	0.06%	0.06%	0.06%	0.13%	0.17%	0.17%
η, %	0.13	0.01	0.01	0.01	0.01	4.92	1.07
k	1	2	2	2	2	2	2
$N_{\mathcal{T}_k}$	165249	312235	419430	282117	77370	51096	47488
N_{tot}							
N_{max}							
CPU total	27.5s	675.9s	936.8s	555.8s	122.9s	33.8s	26.9s
CPU (definition)	5.2s	8.8s	9.7s	7.4s	7.6s	6.3s	6.1s
CPU (resolution)	20.8s	29.6s	42.3s	37.4s	11.7s	8.5s	7.3s

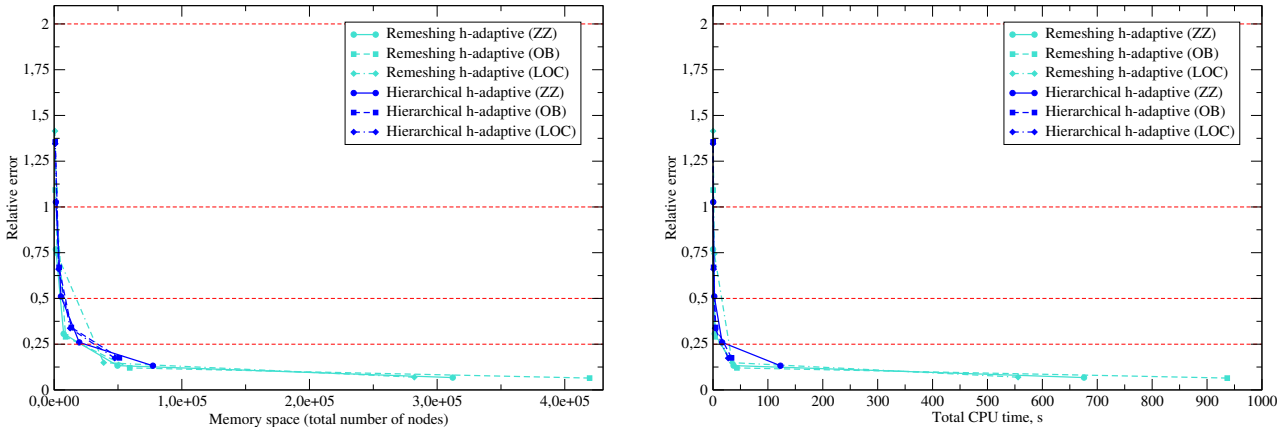

(a) (b)

Figure 23: Mechanical Pellet-Cladding Interaction / Adjusted-ratio refinement: (a) Relative error vs number of nodes N_{tot}; (b) Relative error vs total CPU time

Table 6 reports the results obtained for $\epsilon_\Omega = 0.25\%$ while applying the mean adjusted-ratio strategy (Eq.15) on each of the AMR techniques. The minimal elements step reached in this case is equal to $\frac{1}{30} h_{T^0}$ ($k = 2$) whatever the mesh optimality criterion. Hence, the mean adjusted-ratio strategy yields slightly better results, in term of number of nodes as well as CPU time, compared to the fixed-ratio strategy (for which the final minimal elements step is $h_{T_{k,j}} = \frac{1}{32} h_{T^0}$). The evolution of the global relative error with respect to the total number of nodes and to the total CPU time can be observed on Figure 24. A little general improvement of the fixed-ratio strategy results can be observed. But similar tendencies are obtained. The three studied AMR techniques lead to the comparable results in term of the memory space (similar total number of nodes). However, once again the LDC technique clearly appears to be the best approach in term of computational time.

The final local errors, quantitatively evaluated using the η indicator (Eq.32) are reported on Figures 25, 26 and 27 for fixed-ratio, adjusted-ratio and mean adjusted-ratio strategies respectively.

Table 6: Mechanical Pellet-Cladding Interaction / Mean adjusted-ratio refinement

Tolerance 0.25%	Uniform refinement ($h_{T_{1,j}} = 1/32 h_{T^0}$)	Remeshing h-refinement			Hierarchical h-refinement			Local Defect Correction		
		ZZ	OB	LOC	ZZ	OB	LOC	ZZ	OB	LOC
$\|\mathbf{e}^{ex}\|^{rel}_{\mathcal{T}_k}$	0.09%	0.15%	0.15%	0.15%	0.19%	0.19%	0.18%	0.15%	0.15%	0.15%
η, %	0.13	0.44	0.44	0.44	6.85	6.63	1.26	0.69	0.50	0.56
k	1	2	2	2	2	2	2	2	2	2
$N_{\mathcal{T}_k}$	165249	50630	51362	51972	40124	40304	42338	39174	39342	41349
N_{tot}								48434	48682	51412
N_{max}								32020	32268	34998
CPU total	27.5s	58.8s	58.8s	59.6s	25.1s	26.3s	26.6s	15.1s	15.1s	16.6s
CPU (definition)	5.2s	1.1s	1.2s	1.2s	5.5s	5.7s	6.2s	0.6s	0.8s	0.9s
CPU (resolution)	20.8s	8.5s	9.4s	9.3s	9.1s	9.9s	9.4s	5.3s	6.1s	5.9s

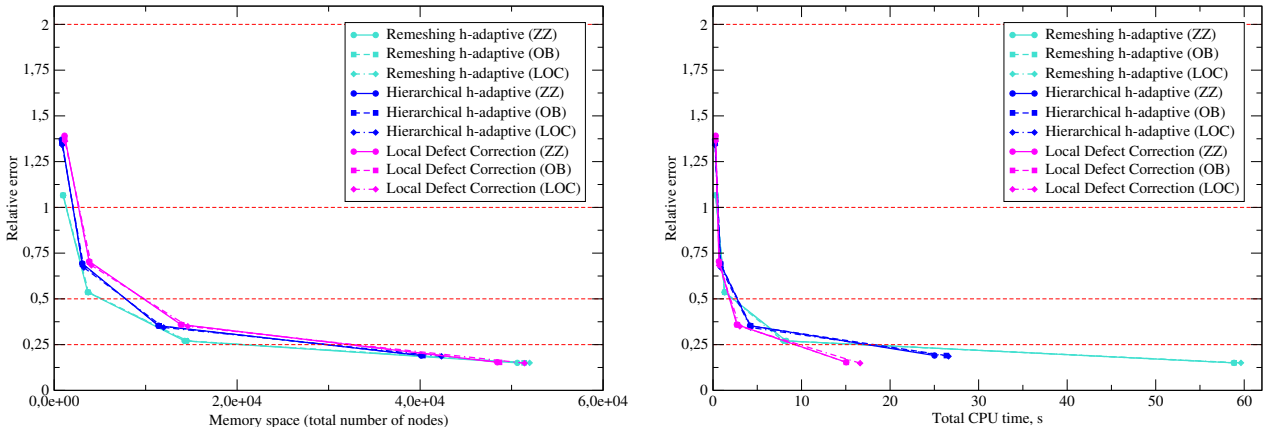

(a) (b)

Figure 24: Mechanical Pellet-Cladding Interaction / Mean adjusted-ratio refinement: (a) Relative error vs number of nodes N_{tot}; (b) Relative error vs total CPU time

Only the LOC criterion guarantees to respect the local accuracy on the required $(100 - \delta)\%$ of the domain (i.e. $\eta \leq \delta$) for all imposed ϵ_Ω values. Moreover, it can be noticed that for the fixed-ratio and mean adjusted-ratio strategies, ZZ and OB mesh optimality criteria result in similar evolution of the η measure. This is due to the fact that for this case, the initial uniform meshes are quite completely uniformly refined leading to equivalent criteria as $\#\mathcal{T}_i = \frac{\mu(\Omega)}{\mu(T^i)}$. As expected, the remeshing h-refinement permits to improve the local accuracy (lower η values) at nearly every case, whatever the optimality criterion. The hierarchical h-adaptive and LDC methods naturally lead to the same order of final local levels of accuracy.

It can be deduced also from this numerical example, that the progressive uniform strategies (fixed-ratio and mean adjusted-ratio) lead to the most competitive results (with a little more improvement while using the mean adjusted-ratio strategy). They permit to better control the mesh-step (and hence the memory space) with respect to the desired accuracy. All AMR techniques lead in this case to similar total number of nodes, with slightly better results for hierarchical h-adaptive method. The multigrid LDC approach has proven to be more efficient in term of CPU time compared to h-refinement strategies for similar final levels of accuracy (global and local errors). Thanks to the LDC technique (local conforming problems separately solved), one gains approximately 40 to 50% of the total runtime compared to the hierarchical h-refinement (non-conforming relations to be managed) and about 75% compared to the remeshing h-adaptive approach (global conforming meshes to be generated). Moreover, it seems to be in this case the only mesh-step AMR techniques enabling to concurrence in term of CPU time an adapted uniform refinement. Finally, only the LOC mesh optimality criterion enables to precisely control the local

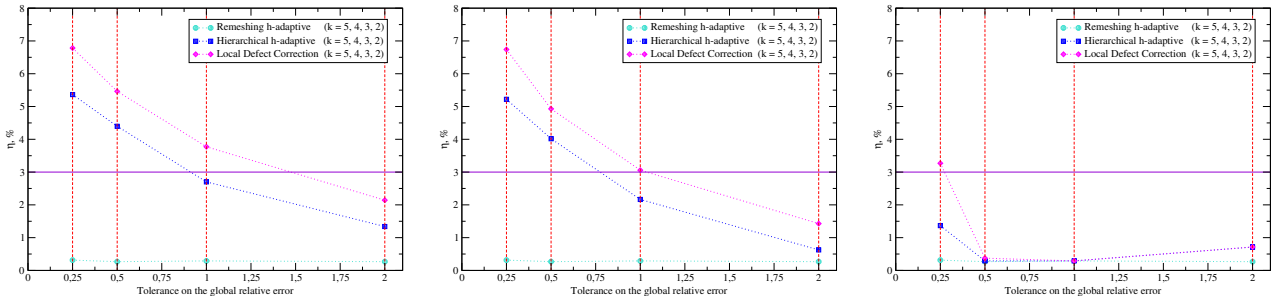

(a) (b) (c)

Figure 25: Mechanical Pellet-Cladding Interaction / Fixed-ratio refinement: (a) ZZ optimality criterion; (b) OB optimality criterion; (c) LOC optimality criterion

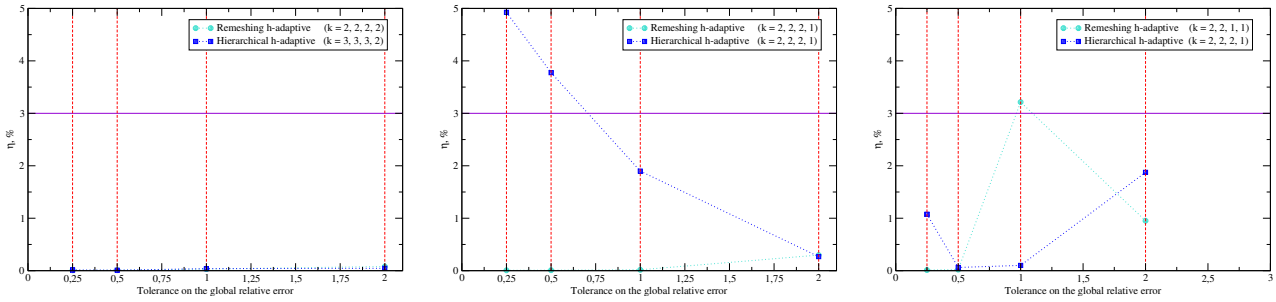

(a) (b) (c)

Figure 26: Mechanical Pellet-Cladding Interaction / Adjusted-ratio refinement: (a) ZZ optimality criterion; (b) OB optimality criterion; (c) LOC optimality criterion

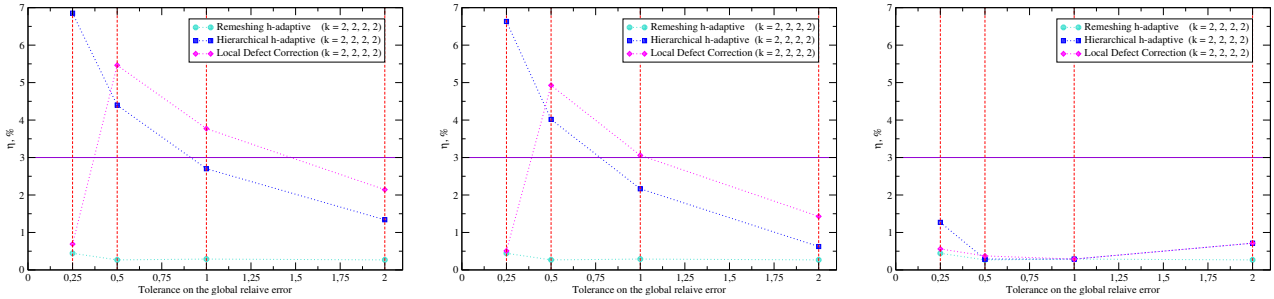

(a) (b) (c)

Figure 27: Mechanical Pellet-Cladding Interaction / Mean adjusted-ratio refinement: (a) ZZ optimality criterion; (b) OB optimality criterion; (c) LOC optimality criterion

error. Indeed, in this case, the OB criterion is not enough precise locally, maybe due to the presence of local singularity.

4.5 Further remarks and suggestions

Within the limits of this study, the fixed-ratio strategy with $\beta_{T^i} = 2$ has shown to be the most robust refinement strategy. As already discussed, this strategy permits to progressively improve the mesh and to precisely reach the required level of accuracy. Nevertheless, the possibility of the adjusted scaling factor to achieve the imposed precision in less remeshing steps seems to be very attractive and a promising feature. However, the estimated values of the adjusted scaling factors may be inappropriate and their direct application may sometimes lead to irrelevant refinement. Generally, the regions to be refined are properly detected whatever the mesh optimality criterion used (especially with OB and LOC criteria), but it is the computation of an optimal element-step distribution (see Eq.13), obtained assuming the convergence rule (Eq.14) which may be

questioned. Indeed, two important hypotheses were made: the first one states the independence of the constant C_{T^i} to the mesh-step while the second one claims the accordance of the local convergence order p to the one obtained globally (order p here). It seems natural that constant C_{T^i} may depend on the mesh size as the constant of the global *a priori* estimator depends on the domain's measure [51]. This was already suggested in [29]. In addition, it is likely that the local convergence order may change, for example near boundaries of the domain or singularities. Therefore, further exploration of *a priori* local error estimators may be greatly interesting in order to improve the formulation of the adjusted scaling factor β_{T^i}. However, preliminary results show that even with a more advanced local *a priori* error estimator, the adjusted-ratio strategy hardly competes the progressive fixed-ratio strategy.

5 Conclusions

In this study, the well-known h-refinement methods have been compared to the multigrid Local Defect Correction method in the context of linear elasticity for quadrangular finite elements. The main distinctions revealed between three mesh refinement methods are summarized as follows:

- The remeshing h-adaptive method requires a complete remeshing of the domain (especially for quadrangular elements), which may quickly become expensive and lead to (very) degenerated elements. Contrariwise, this method is not intrusive and can be easily implemented over the existing routines.

- The hierarchical h-adaptive approach preserves the local character of refinement. Thanks to that, more optimal meshes in terms of number of elements are obtained, but the appearance of the non-conforming nodes is often unavoidable. Additional operations must be carried out to manage the non-conformity relations, which make the method more intrusive and potentially expensive in the CPU time.

  According to obtained results, the hierarchical approach has proved to be less memory space consuming (more optimal in term of generated meshes) than the remeshing approach. The comparison of both approaches in term of total runtime seems depend on the problem. However, both techniques sometimes lead to computations exceeding the time required by an uniform refinement.

- The Local Defect Correction multigrid method permits to ensure the local character of the refinement while circumventing the difficulties related to non-conforming mesh. Hence, it can be implemented in a non-intrusive way (only the pre- and post-processing operations) in any existing software. This technique is really beneficial in CPU time. In some cases it is only the one enabling to reduce the computational cost with regard to an uniform refinement. Even if all generated sub-grids have to be stored in memory, the total number of nodes is finally comparative to the one obtained while using the hierarchical h-adaptive method (where only the last grid has to be kept).

  The really promising results obtained with the local multigrid LDC method opens the way to apply this approach to nonlinear problems. Moreover, this method presents other interesting potentialities, e.g. possibility to change the model, elements type, etc. between levels of refinement.

Furthermore, three mesh optimality criteria have been compared with a special attention dedicated to the local error verification. For both test cases considered in this study, the so-called LOC mesh optimality criterion seems to be the most adapted to precisely control the local error. This is due to the fact that this criterion lies directly on the relative local error verification. However, this criterion may sometimes lead to very refined meshes, useless to respect the global

precision. The so-called ZZ global mesh optimality criterion is often sufficient when only the global mesh optimality is of interest. Finally, the so-called OB criterion appears as a compromise between global and local error control, without precisely controlling the local error.

For both studied test problems, one can conclude that the progressive fixed-ratio strategy is the best trade-off between robustness and cost. It has been proven to be an efficient strategy, in terms of CPU time and memory space, to precisely reach the desired accuracy (global and local errors). However, it may be interesting to further explore the determination of an optimal refinement ratio to improve strategies based on its values. Indeed, this ratio is build from hypotheses on local error estimates that may be discussed.

6 Acknowledgements

This work has been achieved in the framework of the collaboration protocol between CEA (Commissariat à l'Énérgie Atomique et aux Énérgies Alternatives) and the LMA (Laboratoire de Mécanique et d'Acoustique, CNRS, Marseille). The authors are grateful to the PLEIADES project, financially supported by the CEA, EDF (Eléctricité de France) and FRAMATOME, that founded this research work.

References

[1] S. Ghosh and S.K. Manna. R-adapted Arbitrary Lagrangian-Eulerian Finite Element method in metal-forming simulation. *Journal of Materials Engineering and Performance*, 2(2):271–282, 1993.

[2] W. Cao, W. Huang and R. Russell. An r-adaptive Finite Element method based upon moving mesh PDEs. *Journal of Computational Physics*, 149:221–244, 1999.

[3] L. Demkowicz, Ph. Devloo and J.T. Oden. On an h-type mesh-refinement strategy based on minimization of interpolation errors. *Computer Methods in Applied Mechanics and Engineering*, 53(1):67–89, 1985.

[4] T. Belytschko and M. Tabbara. H-adaptive Finite Element methods for dynamic problems, with emphasis on localization. *International Journal for Numerical Methods in Engineering*, 36(24):4245–4265, 1993.

[5] P. Dìez and A. Huerta. A unified approach to remeshing strategies for Finite Element h-adaptivity. *Computer Methods in Applied Mechanics and Engineering*, 176(1):215–229, 1999.

[6] I. Babuška and B. Szabo. On the rates of convergence of the Finite Element method. *International Journal for Numerical Methods in Engineering*, 18(3):323–341, 1982.

[7] R.R. Salagame and A.D. Belegundu. A simple p-adaptive refinement procedure for structural shape optimization. *Finite Element in Analysis and Design*, 24(3):133–155, 1997.

[8] J. Fish. The s-version of the Finite Element method. *Computers and Structures*, 43(3):539–547, 1992.

[9] Z. Yue and D.H. Robbins. Adaptive superposition of Finite Element meshes in elastodynamic problems. *International Journal for Numerical Methods in Engineering*, 63(11):1604–1635, 2005.

[10] I. Babuška and B.Q. Guo. The h, p and h-p version of the Finite Element method; basis theory and applications. *Advances in Engineering Software*, 15(3):159–174, 1992.

[11] O.C. Zienkiewicz, J.Z. Zhu and N.G. Gong. Effective and practical h–p-version adaptive analysis procedures for the Finite Element method. *International Journal for Numerical Methods in Engineering*, 28(4):879–891, 1989.

[12] H. Askes and A. Rodríguez-Ferran. A combined rh-adaptive scheme based on domain subdivision. formulation and linear examples. *International Journal for Numerical Methods in Engineering*, 51(3):253–273, 2001.

[13] N.G. Zamani and W. Sun. Adaptive r and h-r algorithms for Boundary Elements. *Advances in Engineering Software*, 15(3):241–247, 1992.

[14] S. Ghosh and S. Raju. R–s adapted Arbitrary Lagrangian-Eulerian Finite Element method for metal-forming problems with strain localization. *International Journal for Numerical Methods in Engineering*, 39(19):3247–3272, 1996.

[15] P. Krysl, E. Grinspun and P. Schröder. Natural hierarchical refinement for Finite Element methods. *International Journal for Numerical Methods in Engineering*, 56(8):1109–1124, 2003.

[16] A. Brandt. Rigorous quantitative analysis of multigrid, I: Constant coefficients Two-Level cycle with l_2-norm. *SIAM Journal on Numerical Analysis*, 31(6):1695–1730, 1994.

[17] M.J. Berger and J. Oliger. Adaptive mesh refinement for hyperbolic partial differential equations. *Journal of Computational Physics*, 53(3):484–512, 1984.

[18] A. Brandt. Multi-level adaptive solutions to boundary-value problems. *Mathematics of Computation*, 31(138):333–390, 1977.

[19] W. Hackbusch. *Local Defect Correction method and Domain Decomposition techniques*, pages 89–113. Springer Vienna, 1984.

[20] S. McCormick. *Fast Adaptive Composite Grid (FAC) Methods: Theory for the Variational Case*, pages 115–121. Springer Vienna, 1984.

[21] Ph. Angot, J-P. Caltagirone and K. Khadra. Une méthode adaptative de raffinement local: la correction du flux à l'interface. *Comptes rendus de l'Académie des sciences. Série 1, Mathématiques*, 315(6):739–745, 1992.

[22] L. Barbié, I. Ramière and F. Lebon. Strategies around the Local Defect Correction multi-level refinement method for three-dimensional linear elastic problems. *Computers and Structures*, 130:73–90, 2014.

[23] W. Ehlers, M. Ammann and S. Diebels. H-adaptive FE methods applied to single- and multiphase problems. *International Journal for Numerical Methods in Engineering*, 54(2):219–239, 2002.

[24] P.G. Ciarlet and P-A. Raviart. Interpolation theory over curved elements, with applications to Finite Element methods. *Computer Methods in Applied Mechanics and Engineering*, 1(2):217–249, 1972.

[25] C. Bernardi and V. Girault. A local regularization operator for triangular and quadrilateral Finite Elements. *SIAM Journal on Numerical Analysis*, 35(5):1893–1916, 1998.

[26] R. Verfürth. A review of a posteriori error estimation and adaptive mesh-refinement techniques. *Wiley, Chichester*, 1996.

[27] O. C. Zienkiewicz and J. Z. Zhu. A simple error estimator and adaptive procedure for practical engineerng analysis. *International Journal for Numerical Methods in Engineering*, 24(2):337–357, 1987.

[28] O. C. Zienkiewicz and J. Z. Zhu. The superconvergent patch recovery and a posteriori error estimates. Part 1: The recovery technique. *International Journal for Numerical Methods in Engineering*, 33(7):1331–1364, 1992.

[29] E. Oñate and G. Bugeda. Mesh optimality criteria for adaptive Finite Element computations. *Engineering Computations*, pages 307–321, 1993.

[30] L-Y. Li, P. Bettess, J.W. Bull, T. Bond and I. Applegarth. Theoretical formulations for adaptive Finite Element computations. *Communications in Numerical Methods in Engineering*, 11(10):857–868, 1995.

[31] P. Ladevèze, J.P. Pelle and P. Rougeot. Error estimation and mesh optimization for classical Finite Elements. *Engineering Computations*, 8:69–80, 1991.

[32] I. Ramière, H. Liu and F. Lebon. Original geometrical stopping criteria associated to multilevel adaptive mesh refinement for problems with local singularities. *Computational Mechanics*, 2019.

[33] H. Liu, I. Ramière and F. Lebon. On the coupling of local multilevel mesh refinement and ZZ methods for unilateral frictional contact problems in elastostatics. *Computer Methods in Applied Mechanics and Engineering*, 323:1–26, 2017.

[34] F. Brezzi and M. Fortin. *Mixed and Hybrid Finite Element method*. Springer-Verlag, Berlin, Heidelberg, 1991.

[35] H.J.C. Barbosa and T.J.R. Hughes. Boundary Lagrange multipliers in Finite Element methods: error analysis in natural norms. *Numerische Mathematik*, 62(1):1–15, 1992.

[36] R. Becker, P. Hansbo and R. Stenberg. A Finite Element method for Domain Decomposition with non-matching grids. *ESAIM: Mathematical Modelling and Numerical Analysis - Modélisation Mathématique et Analyse Numérique*, 37(2):209–225, 2003.

[37] I. Babuška and M. Zlamal. Nonconforming elements in the Finite Element method with penalty. *SIAM Journal on Numerical Analysis*, 10(5):863–875, 1973.

[38] G.F. Carey. Nonconforming elements, patch tests and inter-element constraints. In *Contributions of Mathematical Analysis to the Numerical Solution of Partial Differential Equations*, pages 138–149, Canberra AUS, 1984. Centre for Mathematical Analysis, The Australian National University.

[39] F. Ben Belgacem and Y. Maday. The Mortar Element method for three dimensional Finite Elements. *ESAIM: Mathematical Modelling and Numerical Analysis - Modélisation Mathématique et Analyse Numérique*, 31(2):289–302, 1997.

[40] C. Bernardi, Y. Maday and A. T. Patera. *Domain Decomposition by the Mortar Element method*, pages 269–286. Springer Netherlands, Dordrecht, 1993.

[41] Rong R. Tian and G. Yagawa. Non-matching mesh gluing by meshless interpolation — an alternative to Lagrange multipliers. *International Journal for Numerical Methods in Engineering*, 71(4):473–503, 2007.

[42] K. Khadra, Ph. Angot, J.P. Caltagirone and P. Morel. Concept de zoom adaptatif en architecture multigrille locale; étude comparative des méthodes l.d.c., f.a.c. et f.i.c. *ESAIM: Mathematical Modelling and Numerical Analysis Modélisation Mathématique et Analyse Numérique*, 30(1):39–82, 1996.

[43] M. Anthonissen. Local Defect Correction techniques applied to a combustion problem. In *Domain Decomposition Methods in Science and Engineering*, pages 185–192. Springer Berlin Heidelberg, 2005.

[44] M. Sizov, M.J.H. Anthonissen, R.M.M. Mattheij. Local Defect Correction with compact Finite Difference schemes for convection-diffusion equations. In A. Di Bucchianico, R.M.M. Mattheij and M.A. Peletier, editors, *Progress in Industrial Mathematics at ECMI 2004 (Proceedings 13th European Conference on Mathematics for Industry, Eindhoven, The Netherlands, June 21-25, 2004)*, Mathematics in Industry, pages 523–527, Germany, 2006. Springer.

[45] M.J.H. Anthonissen, B. van't Hof, and A.A. Reusken. A Finite Volume scheme for solving elliptic boundary value problems on composite grids. *Computing*, 61(4):285–305, 1998.

[46] W. Kramer, R. Minero, H.J.H. Clercx and R.M.M. Mattheij. *A Finite Volume Local Defect Correction method for solving the transport equation.* CASA-report. Technische Universiteit Eindhoven, 2006.

[47] G. Kakuba, R.M.M. Mattheij and M.J.H. Anthonissen. Local Defect Correction for the Boundary Element method. *Computer Modeling in Engineering and Sciences*, 15(3):127–136, 2006.

[48] M. Belliard and M. Grandotto. Local zoom computation of two-phase flows in steam generators using a Local Defect Correction method. *Numerical Heat Transfer, Part A: Applications*, 43(2):111–135, 2003.

[49] I. Ramière, Ph. Angot and M. Belliard. A fictitious domain approach with spread interface for elliptic problems with general boundary conditions. *Computer Methods in Applied Mechanics and Engineering*, 196(4):766–781, 2007.

[50] L. Barbié, I. Ramière and F. Lebon. An automatic multilevel refinement technique based on nested local meshes for nonlinear mechanics. *Computers and Structures*, 147:14–25, 2015.

[51] Ph. G. Ciarlet. *Finite Element Method for Elliptic Problems.* Society for Industrial and Applied Mathematics, Philadelphia, PA, USA, 2002.

[52] I. Babuška and W.C. Rheinboldt. A-posteriori error estimates for the Finite Element method. *International Journal for Numerical Methods in Engineering*, 12(10):1597–1615, 1978.

[53] O.C. Zienkiewicz and J.Z. Zhu. The superconvergent patch recovery and a posteriori error estimates. Part 2: Error estimates and adaptivity. *International Journal for Numerical Methods in Engineering*, 33(7):1365–1382, 1992.

[54] P. Ladevèze and D. Leguillon. Error estimate procedure in the Finite Element method and applications. *SIAM Journal on Numerical Analysis*, 20(3):485–509, 1983.

[55] F. Kuss and F. Lebon. Stress based finite element methods for solving contact problems: comparisons between various solution methods. *Advances in Engineering Software*, 40(8):697–706, 2009.

[56] B. Szabo and I. Babuška. Finite Element analysis. *Wiley: New York*, 1990.

[57] P. Díez and A. Huerta. A unified approach to remeshing strategies for Finite Element h-adaptivity. *Computer Methods in Applied Mechanics and Engineering*, 176(1):215–229, 1999.

[58] G. Bugeda and J. Oliver. A general methodology for structural shape optimization problems using automatic adaptive remeshing. *International Journal for Numerical Methods in Engineering*, 36(18):3161–3185, 1993.

[59] CEA. Cast3m, 2019.

[60] D. Fournier, R. Herbin, and R. Le Tellier. Discontinuous Galerkin Discretization and *hp*-refinement for the resolution of the neutron transport equation. *SIAM Journal on Scientific Computing*, 35:A936–A956, 2013.

[61] V. Faucher, F. Casadei, G. Valsamosand M. Larcher. High resolution adaptive framework for fast transient fluid-structure interaction with interfaces and structural failure – application to failing tanks under impact. *International Journal of Impact Engineering*, 127:62–85, 2018.

[62] W. Rachowicz L. Demkowicz, J. Kurtz, D. Pardo, M. Paszynsk, and A. Zdunek. *Computing with hp-adaptive finite elements: three dimensional elliptic and Maxwell problems with applications, Vol.1*. Chapman and Hall, 2007.

[63] R. H. Nochetto and A. Veeser. *Primer of Adaptive Finite Element Methods*. Springer Berlin Heidelberg, 2012.

[64] P. Cavin, A. Gravouil, A. A. Lubrecht and A. Combescure. Efficient FEM calculation with predefined precision through automatic grid refinement. *Finite Elements in Analysis and Design*, 41(11-12):1043–1055, 2005.

[65] I. Ramière. Convergence analysis of the q1-Finite Element Method for elliptic problems with non-boundary-fitted meshes. *International Journal for Numerical Methods in Engineering*, 75(9):1007–1052, 2008.